Intestinal immunological events of acute and resolved SARS-CoV-2 infection in non-human primates

Stéphane Hua, Krishna Latha, Romain Marlin, Keltouma Benmeziane, Laetitia Bossevot, Sébastien Langlois, Francis Relouzat, Nathalie Dereuddre-Bosquet, Roger Le Grand, Mariangela Cavarelli

ARTICLE

Intestinal immunological events of acute and resolved SARS-CoV-2 infection in non-human primates

Stéphane Hua [†], Krishna Latha [†], Romain Marlin, Keltouma Benmeziane, Laetitia Bossevot, Sébastien Langlois, Francis Relouzat, Nathalie Dereuddre-Bosquet, Roger Le Grand and Mariangela Cavarelli [✉]

SARS-CoV-2 infection has been associated with intestinal mucosal barrier damage, leading to microbial and endotoxin translocation, heightened inflammatory responses, and aggravated disease outcomes. This study aimed to investigate the immunological mechanisms associated with impaired intestinal barrier function. We conducted a comprehensive analysis of gut damage and inflammation markers and phenotypic characterization of myeloid and lymphoid populations in the ileum and colon of SARS-CoV-2-exposed macaques during both the acute and resolved infection phases. Our findings revealed a significant accumulation of terminally differentiated and activated CD4+ and CD8+ T cells, along with memory B cells, within the gastrointestinal tract up to 43 days after exposure to SARS-CoV-2. This robust infection-induced immune response was accompanied by a notable depletion of plasmacytoid dendritic cells, myeloid dendritic cells, and macrophages, particularly affecting the colon during the resolved infection phase. Additionally, we identified a population of CX3CR1^{Low} inflammatory macrophages associated with intestinal damage during active viral replication. Elevated levels of immune activation and gut damage markers, and perturbation of macrophage homeostasis, persisted even after the resolution of the infection, suggesting potential long-term clinical sequelae. These findings enhance our understanding of gastrointestinal immune pathology following SARS-CoV-2 infection and provide valuable information for developing and testing medical countermeasures.

Mucosal Immunology (2024) 17:25–40; https://doi.org/10.1016/j.mucimm.2023.10.001

INTRODUCTION

COVID-19 is caused by the Severe Acute Respiratory Syndrome Coronavirus-2 (SARS-CoV-2) and is well known for airborne transmission with maximal impact on the respiratory system[1–3]. The disease may progress in the majority of infected individuals with mild symptoms or asymptomatically at the peak of viral replication. However, 6–14 days after the onset of symptoms, some individuals encounter late severe manifestations involving acute respiratory distress syndrome and poorer prognosis, including fatal outcomes[4–7]. Disease severity depends on the balance between host immune response, viral replication, and tissue and organ damage. In severe COVID-19, deregulated hyperinflammation and hyperactivated immune responses can occur, characterized by very high levels of cytokines and pro-inflammatory biomarkers and increase complement activation[8–10].

It is well established that COVID-19 is not only a respiratory tract disease but also impairs the functions of other organs[11–13]. A disruption of the crosstalk between the lung and the gut has been implicated as a driver of severity during diseases transmitted through the respiratory tract[14,15]. The virus primarily infects the host lung cells, and viral particles are preferentially released apically by the airway cells. Thus, the released SARS-CoV-2 virus removed by mucociliary clearance may access the gastrointestinal (GI) tract *via* luminal exposure. In addition, droplets carrying the virus can be swallowed and pass to the GI tract. Indeed, several studies indicated the GI tract as a possible entry or interaction site of SARS-CoV-2[11,16,17], leading to complex immune activation, digestive symptoms, altered microbiome, and development of severe COVID-19. Both ACE2 and TMPRSS2, the receptors required for infection, are highly expressed in the GI tract, particularly by intestinal epithelial cells[18], and enterocyte infection has been repeatedly demonstrated[16,19–22]. A clinical output associated with viral exposure of the GI tract is the rectal shedding of the virus in the stool or in rectal fluids, which was observed also with other coronaviruses such as MERS[23] or SARS-CoV[24,25] and with Influenza virus[26,27]. Over 50% of SARS-CoV-2 infected patients had a detectable rectal viral load, and persistent viral shedding up to 17 days post-infection was reported[16,28]. In addition, the early appearance of gastrointestinal perturbations such as nausea, vomiting, abdominal pain, and diarrhea has been documented in almost 30% of COVID-19 patients during the onset of the disease[29–31] and has been linked to a worse clinical outcome[32–34]. Persistent GI symptoms were observed in patients 5 months after SARS-CoV-2 infection[35], and infected individuals had a higher likelihood of

Université Paris-Saclay, Inserm, CEA, Center for Immunology of Viral, Auto-immune, Hematological and Bacterial diseases (IMVA-HB/IDMIT), Fontenay-aux-Roses & Le Kremlin-Bicêtre, France. ✉ email: mariangela.cavarelli@cea.fr

Received: 19 July 2023 Accepted 4 October 2023
Published online: 10 October 2023

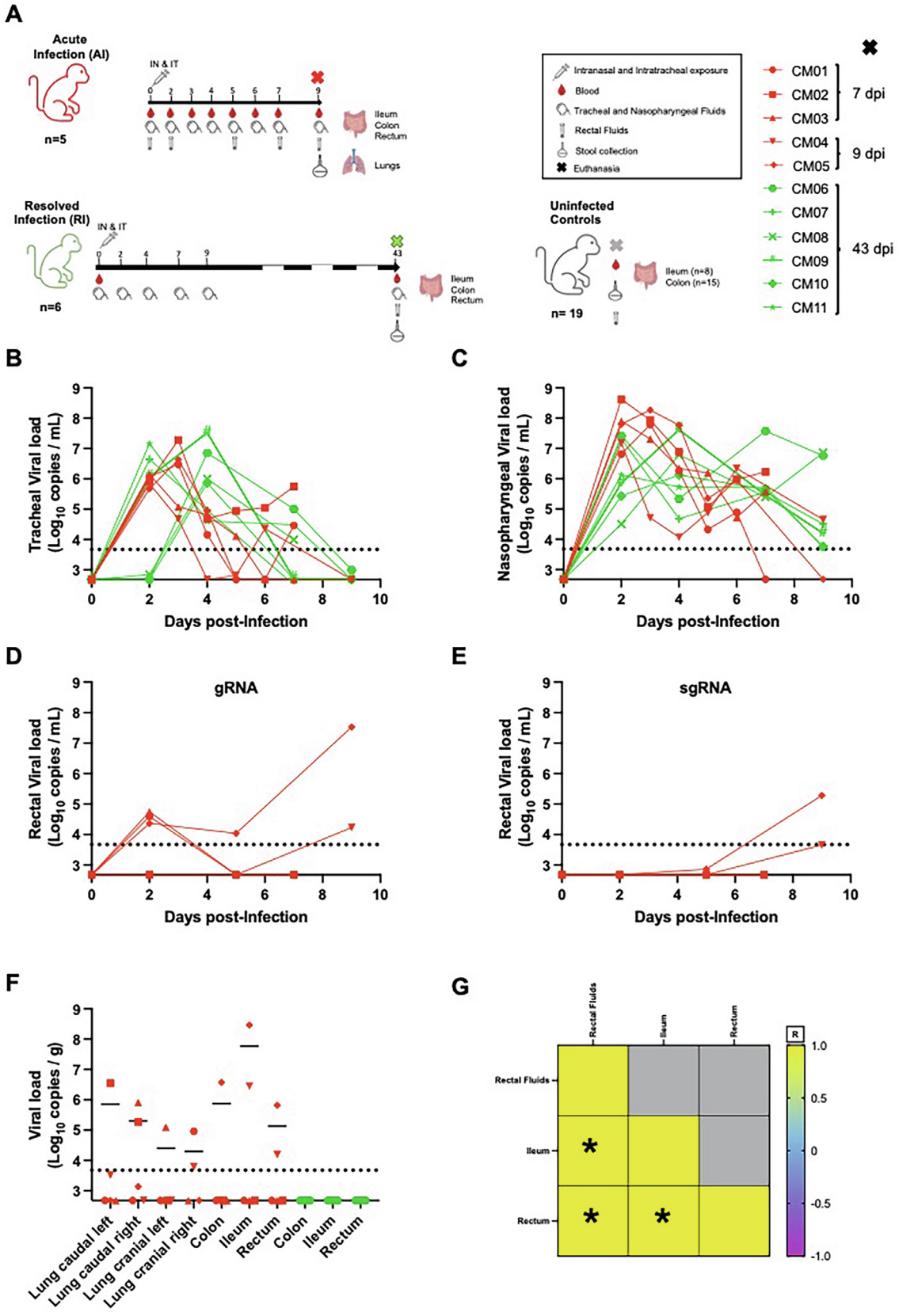
A
Acute Infection (AI)
n=5
IN & IT
Ileum
Colon
Rectum
Lungs
Resolved Infection (RI)
n=6
Uninfected Controls
n= 19
Ileum (n=8)
Colon (n=15)
Intranasal and Intratracheal exposure
Blood
Tracheal and Nasopharyngeal Fluids
Rectal Fluids
Stool collection
Euthanasia
CM01
CM02
CM03
7 dpi
CM04
CM05
9 dpi
CM06
CM07
CM08
CM09
CM10
CM11
43 dpi
B
Tracheal Viral load (Log10 copies / mL)
Days post-Infection
C
Nasopharyngeal Viral load (Log10 copies / mL)
Days post-Infection
D
gRNA
Rectal Viral load (Log10 copies / mL)
Days post-Infection
E
sgRNA
Rectal Viral load (Log10 copies / mL)
Days post-Infection
F
Viral load (Log10 copies / g)
Lung caudal left
Lung caudal right
Lung cranial left
Lung cranial right
Colon
Ileum
Rectum
Colon
Ileum
Rectum
G
Rectal Fluids
Ileum
Rectum
R
1.0
0.5
0
-0.5
-1.0

developing GI disorders within one year after infection compared to uninfected ones[36]. Patients with severe COVID-19 had a higher incidence of GI symptoms compared with patients with a mild form of the disease[4,37]. Although not emphasized, similar symptoms have also been reported during prior coronavirus outbreaks, such as MERS and SARS[31,38].

Although the underlying pathophysiology of GI involvement during SARS-CoV-2 infection is not fully understood, a loss of the intestinal barrier integrity[32,39] along with increased levels of intestinal fatty acids binding protein (iFABP)[40], a marker of intestinal injury, has been observed. The disruption of the intestinal barrier could activate innate and adaptive immune cells, which in turn release proinflammatory cytokines into the circulatory system, leading to systemic inflammation[41,42]. The mucosal inflammatory response increases intestinal permeability resulting in positive feedback and allows various bacterial antigens and toxins to enter the bloodstream, further complicating the recovery of COVID-19 patients. One piece of evidence that SARS-CoV-2 causes an inflammatory response in the gut is the elevated levels of fecal calprotectin (FC) in infected patients[43,44]. In subjects with diarrhea as a symptom, the FC concentrations were elevated, and higher serum IL-6 levels have been reported[43]. To date, while very few studies have analyzed the immunological events occurring in the intestinal compartment of individuals exposed to SARS-CoV-2, they revealed an altered distribution of some immune cell subsets[45–47]. However, none of those studies described a functional link between the changes in frequency or function of immune cells and the perturbation of the intestinal barrier.

By using a non-human primate (NHP) model of SARS-CoV-2 respiratory infection this study aimed to analyze the related intestinal immune cell changes and to assess whether these defects were restored after the resolution of infection. Moreover, we addressed whether those immunological perturbations were linked to an altered intestinal barrier. Our results highlight the loss of the intestinal macrophage's homeostasis as a potential force contributing to the disruption of gut functions.

RESULTS

Rectal shedding of the virus during the acute phase of infection is observed in macaques exposed to SARS-CoV-2

Eleven adult cynomolgus macaques, belonging to two independent study cohorts, were exposed to either 10^5 or 10^6 plaque-forming units (PFUs) of SARS-CoV-2 (Table S1) by a combination of intra-nasal and intratracheal routes. The study was concluded at either 7 – 9 days post-infection (dpi) (n = 5, acute infection group, AI) or 43 dpi (n = 6, resolved infection group, RI) (Fig. 1A). All animals had high viral loads in tracheal and nasopharyngeal fluids as early as 2 dpi, with a peak between 2 and 4 dpi, irrespective of the viral inoculum dose (Fig. 1B, C). Thereafter, the viral load progressively decreased, and most animals had undetectable tracheal viral loads by 9 dpi. The overall viral shedding, as measured by the Area Under the Curve (AUC) from 0 to 9 dpi, did not change in AI versus RI groups ($p = 0.6623$ and $p = 0.1255$, respectively, for tracheal and nasopharyngeal viral load; Supplementary Fig. 1A, B). Infected macaques exhibited mild clinical symptoms (Supplementary Fig. 1C, D), recapitulating an asymptomatic or mildly symptomatic disease seen in the large majority of patients[48–50]. No gastrointestinal symptoms were registered. Transient blood lymphopenia was observed at 2 dpi ($2.2 \times 10^3 \pm 1.5 \times 10^3$ cells/µL *vs.* $4.7 \times 10^3 \pm 1.9 \times 10^3$ cells/µL at baseline; Supplementary Fig. 1E).

Rectal fluids were available at follow-up only from animals assigned to the acute infection group. The viral kinetics profile in rectal swabs as assessed by genomic RNA was nonetheless less consistent than in tracheal and nasal swabs, with 4 macaques displaying a detectable rectal viral load at 2 dpi and 2 out of 5 animals experiencing viral shedding up to 9 dpi (Fig. 1D). Replicative virus was detected by sub-genomic RNA analysis at 9 dpi in the same 2 animals (Fig. 1E). To determine the duration of rectal viral shedding in a larger and independent cohort, viral load was assessed in rectal fluids from 32 macaques additionally exposed to the same Wuhan SARS-CoV-2 strain. 25% of infected animals showed sustained viral loads in their rectal fluid up to 10 dpi, and 16.7% had a positive rectal viral load for more than 2 weeks, when the tracheal and nasal viral loads were still detectable in only 0% and 8% of animals, respectively (Supplementary Fig. 1F). At euthanasia, the rectal viral load was below the lower limit of detection (476 copies/mL) in all 6 RI animals.

Thus, the data indicate an interaction of SARS-CoV-2 with the macaque's GI tract following an airway infection. In accordance with the results obtained on analyzed fluids, examination of the tissues collected at euthanasia revealed detectable viral RNA load in the lungs from up to 4 AI animals and confirmed that SARS-CoV-2 was detectable in the GI tract (either colon, ileum, or rectum) exclusively from AI animals with prolonged rectal viral shedding (Fig. 1F). Interestingly, the animals having a higher viral load in the GI tract are not the same as those with the highest viral load in the lung and tracheal swabs. At euthanasia of AI animals, viral load in the ileum positively correlated with both rectal viral load (r = 1.0, $p = 0.05$) and viral load in rec-

Fig. 1 Establishment of SARS-CoV-2 infection. (A) Study design. Eleven macaques were exposed to SARS-CoV-2 virus by the intratracheal and intranasal routes. Five animals were assigned to the acute infection (AI) group and six to the resolved infection (RI) group. Samples were collected at the indicated day post-infection (dpi). Tissues were collected at euthanasia from AI, RI, and negative control animals (n = 19 in total, in gray) not exposed to the virus. Genomic viral RNA load was measured by RT-qPCR in (B) the tracheal and (C) the nasopharyngeal fluids on the specified dpi. Genomic (D) and sub-genomic (E) rectal viral load from AI animals. (F) Viral load from each of the given tissues obtained at the euthanasia of AI and RI animals. The limit of detection was estimated at 4.76×10^2 copies/mL, and the limit of quantification was estimated at 4.76×10^3 copies/mL (dotted horizontal line in B, C, D, and E). (G) Spearman's correlation matrix using multiple variable table between the viral titer in rectal swabs and in intestinal tissues at euthanasia of AI animals. The correlation matrix is represented as a double gradient map with yellow indicating the highest positive correlation of 1 and pink indicating the highest negative correlation of −1. Significant q values are indicated in each panel.

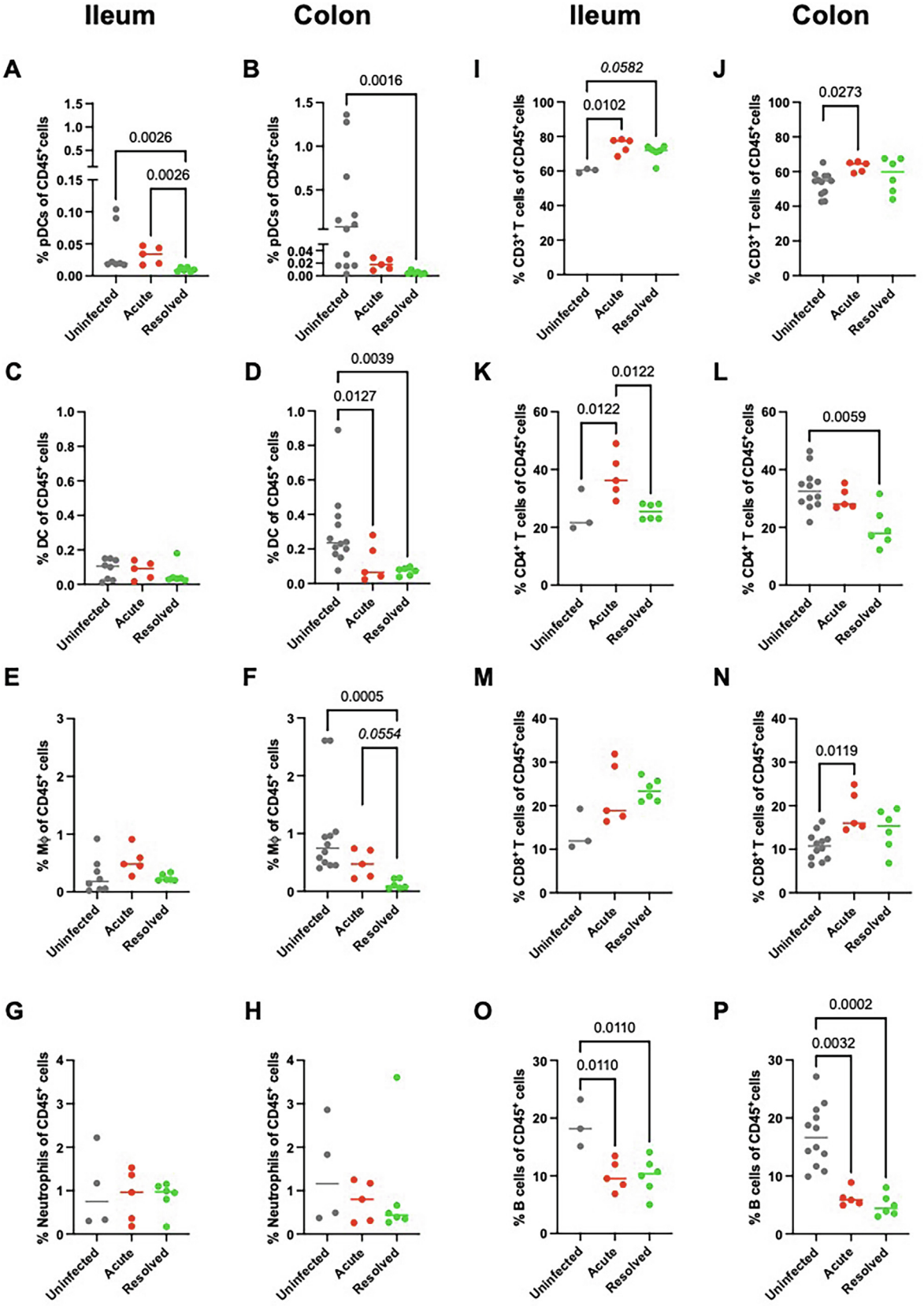
Ileum
Colon
Ileum
Colon
A
B
I
J
% pDCs of CD45+cells
0.0026
0.0026
0.0016
% CD3+ T cells of CD45+cells
0.0582
0.0102
0.0273
C
D
K
L
% DC of CD45+ cells
0.0039
0.0127
% CD4+ T cells of CD45+cells
0.0122
0.0122
0.0059
E
F
M
N
% Mϕ of CD45+ cells
0.0005
0.0554
% CD8+ T cells of CD45+cells
0.0119
G
H
O
P
% Neutrophils of CD45+ cells
% B cells of CD45+cells
0.0110
0.0110
0.0002
0.0032
Uninfected
Acute
Resolved

tal fluid (r = 1.0, p = 0.05) (Fig. 1G). Overall, these results confirmed 43 dpi as a phase of "resolved" viral infection.

Differences in the immune response in the small and large intestines following systemic SARS-CoV-2 infection

To characterize the immune response occurring in the GI tract during the acute and resolved phases of infection, lamina propria mononuclear cells (LPMCs) were isolated from the ileum and colon of uninfected controls and SARS-CoV-2 exposed AI and RI animals (Fig. 1A and Table S2). Immunophenotypic analysis was performed by flow cytometry to identify changes in myeloid and lymphoid immune populations. The gating strategies are shown in Supplementary Figs. 2–4. CD11c$^-$ CD123$^+$ pDCs were significantly reduced in the *lamina propria* of both the ileum and the colon of RI animals compared to uninfected controls (q = 0.0026 and q = 0.0016, respectively, Fig. 2A, B), analogous to changes described in the GI tissues of COVID-19 patients[46]. pDCs were also present in lower numbers in the ileum of RI animals than in AI animals (q = 0.0026). On the contrary, CD11c$^+$ CD123$^-$ CD64$^-$ myeloid DCs (DCs) (Fig. 2C, D) and CD64$^+$ macrophages (Mφs) (Fig. 2E, F) were significantly reduced in the colon of RI animals compared to controls (q = 0.0039 and q = 0.0005, respectively) but not in the ileum. A tendency toward a reduced frequency of colonic Mφs in RI versus AI animals was also observed (q = 0.0554), whereas colonic DCs were significantly reduced in AI animals compared to controls (q = 0.0127). No major changes were observed in the frequency of either total neutrophils (Fig. 2G, H) or neutrophil subsets (i.e. immature, mature, and pre-neutrophil, Supplementary Fig. 5) among the three cohorts at both intestinal sites.

CD3$^+$ T lymphocytes were significantly upregulated during the acute infection phase in both the ileum and the colon (q = 0.0102 and q = 0.0273, respectively, Fig. 2I, J), however, the observed increased frequency was not due to the same T-cell population (Fig. 2K–N). Indeed, it was driven by CD4$^+$ T cells in the ileum (q = 0.0122 compared to both uninfected and RI animals) (Fig. 2K) and by CD8$^+$ T cells in the colon (q = 0.0119 comparing AI versus uninfected animals) (Fig. 2 N). Conversely, CD8$^+$ T cells were enriched in the ileum of RI animals compared to controls, although not reaching a statistically significant difference after multiple correction was applied (p = 0.0280, and q = 0.0882, Fig. 2M). B lymphocytes did not show the same trend as both AI and RI animals showed significantly reduced frequency of B cells compared to controls in both the ileum (q = 0.011, Fig. 2O) and the colon (q = 0.0032 and q = 0.0002, respectively, Fig. 2P).

Our results indicate that intestinal tissues of animals exposed to SARS-CoV-2 are characterized by changes in the proportion of various immune cell subsets, some of which persist or are further exacerbated after the resolution of infection. Those changes were only partially consistent between the ileum and the colon, indicating that SARS-CoV-2 differently affects the immune response along the intestinal tract.

Following SARS-CoV-2 infection, a memory lymphocyte response is observed in the GI tract

To further characterize subsets of the T and B lymphocytes, we focused on the activation status and memory development in the ileum and colon. We analyzed the expression of HLA-DR and CD69, two T-cell activation markers that are commonly elevated on CD8$^+$ T cells during viral infection, such as HIV-1[51–53]. The percentage of HLA-DR$^+$ CD4$^+$ and HLA-DR$^+$ CD8$^+$ T cells was significantly increased in both the ileum and the colon of RI animals compared to both uninfected (q = 0.039 and q = 0.0042 for ileum and colon CD4$^+$ T cells, respectively; q = 0.0072 and q < 0.0001 for ileum and colon CD8$^+$ T cells, respectively) and AI animals (q = 0.0064 and q = 0.0104 for ileum and colon CD4$^+$ T cells, respectively; q = 0.0101 and q = 0.0630 for ileum and colon CD8$^+$ T cells, respectively) (Fig. 3A, B). The frequency of CD69$^+$ CD4$^+$ and CD69$^+$ CD8$^+$ T cells did not vary significantly over the course of infection, except for a significant reduction in the frequency of CD69$^+$ CD4$^+$ T cells in the ileum of RI group (q = 0.0054 compared to both uninfected and AI animals) (Fig. 3A). In addition, an increased frequency of HLA-DR$^+$ CD69$^+$ CD4$^+$ T cells was observed in the colon of RI animals compared to both uninfected (q = 0.0005) and AI macaques (q = 0.0446) whereas HLA-DR$^+$ CD69$^+$ CD8$^+$ T cells were increased in the colon of both AI and RI macaques compared to uninfected controls (q = 0.0057 and q = 0.0002, respectively) (Supplementary Fig. 6).

We used CD95 and CD28 markers to discriminate naïve (CD95$^-$) from memory (CD95$^+$) T lymphocytes, while the CD45RA expression by memory cells (terminally differentiated effector memory T cells, TEMRA, CD95$^+$ CD28$^-$ CD45RA$^+$) is considered to be a marker of end-stage differentiation[54] (Supplementary Fig. 4). In the ileum, most of the lymphocyte memory subsets were unchanged, with the exception of the TEMRA CD8$^+$ T cells, which increased in frequency in the resolved phase compared to the acute phase (q = 0.005) (Fig. 3C, D). In the colon of RI animals, we observed an increase in the frequency of both CD4$^+$ CD95$^+$ CD28$^+$ T cells (q = 0.0017 to uninfected) and CD8$^+$ CD95$^+$ CD28$^+$ T cells (q = 0.0447 compared to uninfected and q = 0.0249 compared to AI), along with a concomitant decrease of CD95$^-$ CD28$^+$ naïve CD4$^+$ T cells (q = 0.0011 compared to uninfected) (Fig. 3 E, F). Additionally, TEMRA CD4$^+$ T cells of the colon were significantly downregulated in AI animals

Fig. 2 Myeloid and lymphocyte populations in the ileum and the colon of macaques exposed to SARS-CoV-2. Lamina propria mononuclear cells were isolated from the ileum and the colon collected at the euthanasia from uninfected controls (8 and 12, respectively, and subjected to specific cell immunophenotyping as described in Table S2), acute (n = 5) and resolved (n = 6) SARS-CoV-2 infection groups. Shown is the frequency among total leucocytes (CD45$^+$ cells) of plasmacytoid DCs (A and B), myeloid DCs (C and D), macrophages (E and F), neutrophils (G and H), CD3$^+$ T cells (I and J), CD4$^+$ T cells (K and L), CD8$^+$ T cells (M and N) and B cells (O and P) from the ileum and the colon, respectively. The mean ± the SD are plotted. Kruskal-Wallis test with FDR correction was applied to the data. Significant q values are indicated in each panel.

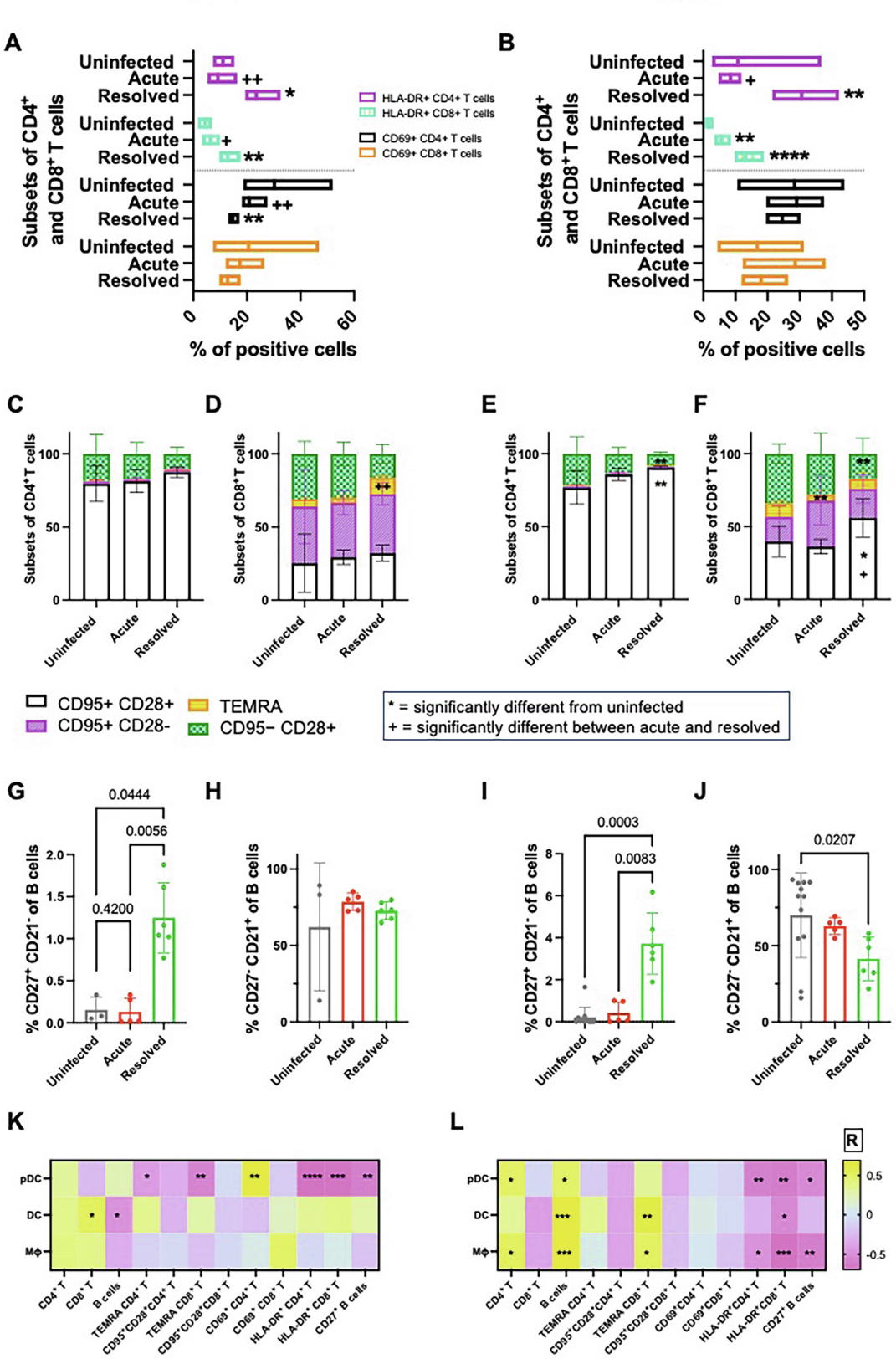
Ileum
Colon
A
B
Subsets of CD4+ and CD8+ T cells
Uninfected
Acute
Resolved
HLA-DR+ CD4+ T cells
HLA-DR+ CD8+ T cells
CD69+ CD4+ T cells
CD69+ CD8+ T cells
% of positive cells
C
D
E
F
Subsets of CD4+ T cells
Subsets of CD8+ T cells
CD95+ CD28+
CD95+ CD28-
TEMRA
CD95− CD28+
* = significantly different from uninfected
+ = significantly different between acute and resolved
G
H
I
J
% CD27+ CD21- of B cells
% CD27- CD21+ of B cells
0.0444
0.0056
0.4200
0.0003
0.0083
0.0207
K
L
R
pDC
DC
Mϕ
CD4+ T
CD8+ T
B cells
TEMRA CD4+ T
CD95+CD28+CD4+ T
TEMRA CD8+ T
CD95+CD28+CD8+ T
CD69+ CD4+ T
CD69+ CD8+ T
HLA-DR+ CD4+ T
HLA-DR+ CD8+ T
CD27+ B cells

compared to both controls and RI animals (q = 0.0040) (Fig. 3E and Supplementary Fig. 7), and TEMRA CD8$^+$ T cells were downregulated in AI animals compared to controls (q = 0.0081; Fig. 3F). B cells were divided into naïve (CD27$^-$ CD21$^+$), resting memory (CD27$^+$ CD21$^+$), activated memory (CD27$^+$ CD21$^-$), and tissue-like memory (CD27$^-$ CD21$^-$) on the basis of CD21 and CD27 expression (Supplementary Fig. 4). CD27$^+$ CD21$^-$ memory B cells were upregulated in the resolved phase of infection in both the ileum (q = 0.0444 compared to uninfected and q = 0.0056 compared to AI) and colon (q = 0.0003 compared to uninfected and q = 0.0083 compared to AI) (Fig. 3G, I) whereas CD27$^-$ CD21$^+$ naïve B cells were concomitantly reduced only in the colon of RI animals compared to uninfected controls (q = 0.0207) (Fig. 3H, J).

These results demonstrate an accumulation of terminally differentiated and activated CD4$^+$ T, CD8$^+$ T cells and concomitantly of memory B cells in the intestine of RI animals indicating infection-induced reactivity following respiratory tract infection by SARS-CoV-2.

In order to assess the impact of the innate immune cells on the adaptive immune and memory development, correlation analysis was performed between pDCs, DCs, and Mφs with lymphocyte subsets and represented as a heatmap (Fig. 3K, L). Neutrophils were excluded from the heatmap representation as no significant association with any other cell type was observed. In the ileum over the course of infection, pDCs negatively correlated with TEMRA CD4$^+$ (p = 0.0436) and CD8$^+$ T cells (p = 0.0043) as well as with activated HLA-DR$^+$ lymphocytes (p < 0.0001 for HLA-DR$^+$ CD4$^+$ T cells and p = 0.001 for HLA-DR$^+$ CD8$^+$ T cells), whereas a positive association with CD69$^+$ CD4$^+$ T cells was observed (p = 0.0037) (Fig. 3K). A higher number of interactions were observed in the colon instead, where either pDCs, DCs, or Mφs positively correlated with CD4$^+$ T cells (p = 0.0284 for pDCs, and p = 0.0206 for Mφs), B cells (p = 0.0305 for pDCs, p = 0.0026 for DCs, and p = 0.0009 for Mφs), and TEMRA CD8$^+$ T cells (p = 0.0061 for DCs, and p = 0.0232 for Mφs), while simultaneously having a negative impact on the HLA-DR$^+$ CD4$^+$ T cells (p = 0.0055 for pDCs, and p = 0.0278 for Mφs), HLADR$^+$ CD8$^+$ T cells (p = 0.0031 for pDCs, p = 0.0112 for DCs, and p = 0.0006 for Mφs) and memory B cells (p = 0.0175 for pDCs, and p = 0.0052 for Mφs) (Fig. 3L).

These results suggest that while similar interactions between pDCs and adaptive/memory subsets of cells occurred at both intestinal sites, the loss of colonic DCs and Mφs observed in SARS-CoV-2 exposed animals could influence lymphocyte activation/memory development.

Breakdown of the intestinal epithelial barrier initiates in the acute phase and persists during the resolved phase of SARS-CoV-2 infection

Gut barrier damage has been reported in several cohorts of COVID-19 patients[39,55–57]. To investigate whether the intestinal barrier was perturbed, we analyzed biomarkers of gut barrier permeability and inflammation, in samples (serum or stool) from AI and RI animals compared to uninfected controls. Plasma levels of the intestinal fatty-acid binding protein (iFABP) were significantly higher in the AI group compared to controls (q = 0.0006, Fig. 4A), indicating epithelium and enterocyte damage during the first week post-exposure to SARS-CoV-2[58–60]. At 43 dpi, however, iFABP levels were comparable to those found in macaque not exposed to SARS-CoV-2, suggesting enterocyte turnover. Damage to the intestinal epithelial barrier is expected to lead to increased gut permeability, microbial translocation, and microbial-mediated myeloid inflammation. Indeed, the level of soluble CD14 (sCD14), a monocyte inflammation marker, was greatly increased in RI animals compared to both AI and negative controls (q = 0.0082 and q = 0.0046, respectively, Fig. 4B). Additionally, we observed higher levels of fecal calprotectin (FC), a marker of intestinal inflammation[61,62], in the stools from RI animals compared to the controls (q = 0.0024, Fig. 4C). Moreover, levels of FC positively correlated with levels of sCD14 in the three cohorts (r = 0.7823 p = 0.0003, Fig. 4D). Despite observing no variation in the frequency of neutrophils between the three studied groups (Fig. 2 and Supplementary Fig. 5), a significant positive correlation was observed between the frequency of colonic immature neutrophils in the RI animals and FC levels (r = 0.8407, p = 0.0444, Spearman test, Supplementary Fig. 8), consistent with the knowledge that neutrophils are the primary source of FC[62–64].

In order to examine the cells associated with gut barrier damage, we performed a correlation analysis between levels of iFABP, sCD14, or FC with myeloid and lymphoid cell populations detected in the ileum and colon of AI and RI animals. While in the ileum markers of gut dysfunction were mostly associated with pDCs and CD4$^+$ T cells (Fig. 4E), in the colon a similar association with pDCs but not with T lymphocytes was found. Moreover, a loss of total Mφs was significantly associated with an augmentation of sCD14 (r = -0.6788, p = 0.0253) and a reduction of iFABP levels (r = 0.7699, p = 0.0075) (Fig. 4F).

Altogether, these findings present a picture of long-lasting intestinal barrier perturbation that, albeit initiated during the acute phase, persisted in animals with no detectable viral load after 43 days from the start of the infection.

Fig. 3 Lymphocyte subsets phenotypic analysis and correlation with myeloid cells. (A–B) Percentage of activated HLA-DR$^+$ and CD69$^+$ CD4$^+$ and CD8$^+$ T cells from (A) the ileum and (B) the colon of uninfected, AI, and RI animals. (C-F) Memory subsets of CD4$^+$ and CD8$^+$ T cells from the ileum (C, D) and the colon (E, F) are categorized as central memory (Tcm, CD95$^+$ CD28$^+$), effector memory (Tem, CD95$^+$ CD28$^-$ CD45RA$^-$), effector resident memory (TEMRA, CD95$^+$ CD28$^-$ CD45RA$^+$) and naïve T cells (CD95$^-$ CD28$^+$). (G-J) Percentage of iliac (G) and colonic (I) memory CD27$^+$ CD21$^-$ B cells. Frequency of iliac (H) and colonic (J) naïve CD27$^-$ CD21$^+$ B cells. The mean ± the SD are plotted. Kruskal-Wallis test with FDR correction was applied to the data shown in A–J. Significant q values are indicated in each panel. (K, L) Spearman correlation between myeloid cells (pDCs, DCs, and M□) and lymphocyte subsets over the course of infection (including the acute, resolved, and uninfected groups) are represented as a heatmap for cells in the ileum (K) and the colon (L). The obtained correlation factors (R) are shown on the heatmap with a yellow (positive correlation) to pink (negative correlation) scale. Significant p values are indicated as follows: *$p \leq 0.05$, **$p \leq 0.01$, ***$p \leq 0.001$, **** $p \leq 0.0001$.

Loss of colonic macrophage homeostasis is associated with markers of intestinal barrier disruption

The association we found between colonic Mφs and sCD14/iFABP levels was intriguing because *lamina propria* Mφs have been described to play a pivotal role in the maintenance of the intestinal epithelial barrier[65–67]. Thus, to gain further insight into the immunological mechanisms contributing to gut barrier defects, we phenotypically characterized subsets of colonic Mφs in uninfected, AI, and RI animals using a gating strategy that relies on the expression of CD64, CD14, CX3CR1, and CD11c[68] (Fig. 5A and Supplementary Fig. 2). The reduction observed in the frequency of Mφs among $CD45^+$ leukocytes following SARS-CoV-2 exposure (Fig. 2F and Supplementary Fig. 9A), was mirrored by a similar trend in all the Mφs subsets we analyzed (Supplementary Fig. 9B–D). Additional differences were observed on further examination of Mφs subsets in their relative proportion among total Mφs (Fig. 5 B-D). The majority of $CD64^+$ Mφs from uninfected controls were $CX3CR1^{High}$ (78.16% ± 6.62 of $CX3CR1^{High}$ and 21.28% ±6.87 of $CX3CR1^{Low}$, Fig. 5B), $CD14^-$ (69.53% ± 8.80 of $CD14^-$ and 30.39% ±8.80 of $CD14^+$, Fig. 5C) and mostly mature $CD11c^-$ cells (10.55% ± 9.70 of CD11c+ and 89.44% ± 9.70 of CD11c-, Fig. 5D), a phenotype typical of resident intestinal macrophages[69–71]. Following exposure to SARS-CoV-2 infection, in AI animals we observed a significant reduction of $CX3CR1^{High}$ Mφs (q = 0.0012), and an accumulation of pro-inflammatory $CX3CR1^{Low}$ Mφs (q = 0.001) compared to controls (Fig. 5B), a phenotype partially resembling that described during inflammatory intestinal diseases and early HIV-1 infection[71,72]. Those Mφs displayed a reduced expression of CD14 compared to uninfected controls (q = 0.0186; Fig. 5C) and were mostly mature $CD11c^-$ cells (86% $CD11c^-$ and 13.97% $CD11c^+$ cells) (Fig. 5D). The proportion of $CX3CR1^{High}$ Mφs detected in the colonic lamina propria of RI macaques was restored to levels comparable to uninfected controls (q = 0.2366; Fig. 5B). However, these Mφs showed higher expression of CD14 (q = 0.0151 compared to controls and q = 0.0005 compared to AI animals, Fig. 5C), and CD11c compared to uninfected controls (q = 0.0256, Fig. 5D), indicating their recent recruitment from the periphery. We further analyzed CX3CR1 expression by subsets of $CD14^+$ and $CD14^-$ Mφs (Fig. 5 E–F), as well as immature $CD11c^+$ and mature $CD11c^-$ Mφs (Fig. 5G). The results confirmed a significant accumulation of both $CD14^+$ $CX3CR1^{Low}$ cells (q = 0.0025; Fig. 5E) and $CD14^-$ $CX3CR1^{Low}$ cells (q = 0.0023; Fig. 5F) in AI animals compared to controls. Moreover, $CD11c^-$ $CX3CR1^{Low}$ cells were significantly increased in the colon of AI animals compared to both uninfected controls and RI macaques (q = 0.0008 and 0.0074, respectively; Fig. 5G), whereas $CD11c^-$ $CX3CR1^{High}$ cells were significantly reduced in the colon of both AI and RI animals compared to controls (q = 0.0033 and 0.0532, respectively; Fig. 5G). Interestingly, fractalkine/CX3CL1, the ligand of CX3CR1

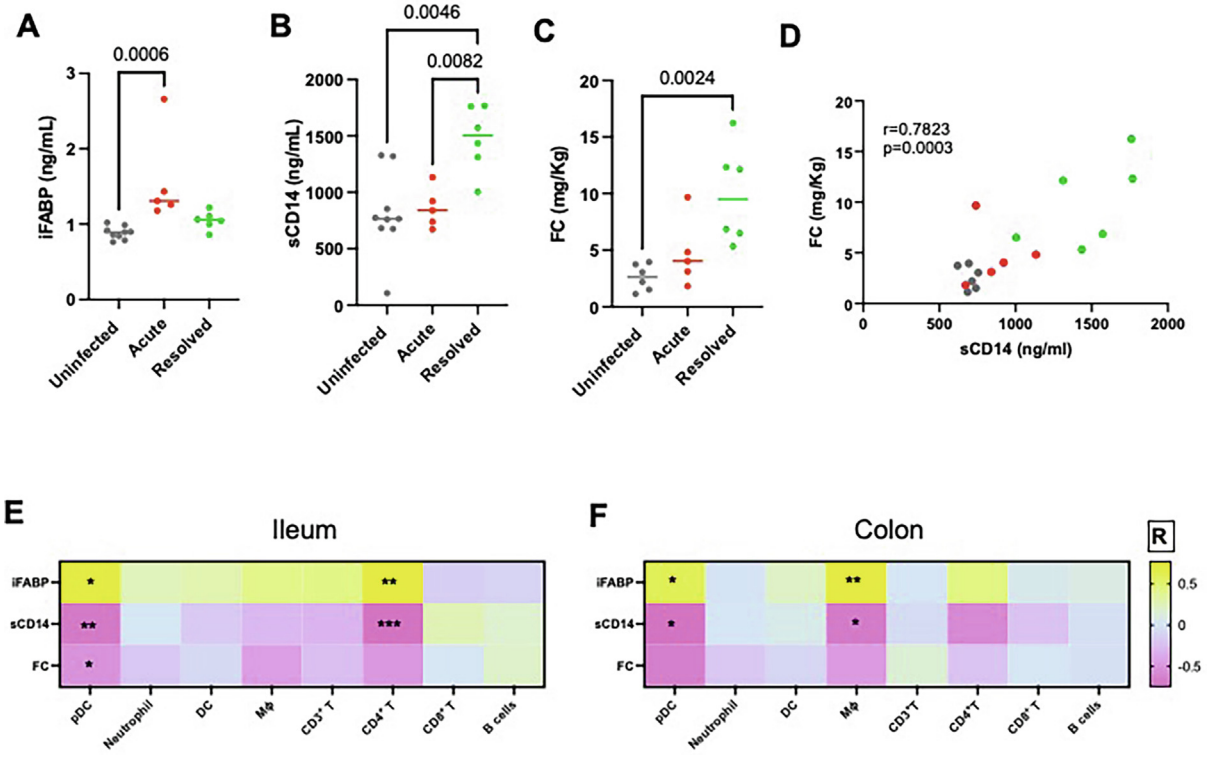

Fig. 4 Markers of intestinal barrier damage over the course of SARS-CoV-2 infection. (A–B) The serum concentration of iFABP (A), and sCD14 (B), from uninfected controls (n = 8 or 9), acute (n = 5), and resolved (n = 6) SARS-CoV-2 infection groups. (C) Levels of fecal calprotectin (FC) from uninfected controls (n = 6), acute (n = 5), and resolved (n = 6) SARS-CoV-2 infection groups. The mean is shown. Kruskal-Wallis test with FDR correction was applied to the data. (D) Spearman correlation between the FC levels and the concentration of sCD14 in the serum from uninfected, AI, and RI animals. (E, F) Spearman correlations between the concentration of soluble factors (iFABP, sCD14, and FC) and major immune cell subsets over the course of infection (including AI and RI groups), in the ileum (E) and the colon (F) are represented as a heat map. The obtained correlation factors (R) are shown on the heatmap with a yellow (positive correlation) to pink (negative correlation) scale. Significant p values are indicated as follows: *$p \leq 0.05$, **$p \leq 0.01$, ***$p \leq 0.001$, ****$p \leq 0.0001$.

known to have pro-inflammatory functions[73], was significantly upregulated in the serum of RI animals compared to uninfected controls (q = 0.0031, Supplementary Fig. 10A) and was linked to the loss of total colonic Mφ (r = −0.6291, $p = 0.0138$, Supplementary Fig. 10B).

We then examined the potential association between markers of gut damage and the proportion of Mφs subsets from uninfected, AI and RI animals. The results are represented as a heatmap in Fig. 5H. iFABP displayed a significant positive correlation with subsets of pro-inflammatory CX3CR1^{Low} Mφ, which is consistent with the accumulation of CX3CR1^{Low} Mφ in AI animals. Conversely, a negative association was found with subsets of CX3CR1^{High} Mφs that populate the colonic lamina propria of uninfected animals. No association between sCD14 and specific Mφs subset was found. However, the augmentation of sCD14 was linked to the loss of CD14$^-$ Mφs (r = −0.5092, $p = 0.026$) and CD11c$^-$ Mφs (r = −0.4662, $p = 0.0383$) rather than CD14$^+$ Mφs and CD11c$^+$ Mφs among CD45$^+$ cells, and was independent of the their CX3CR1 expression (Supplementary Fig. 9E).

Overall, our results indicate that during the phase of active viral replication, colonic Mφs homeostasis is highly compromised. Notably, some phenotypic and presumably functional modifications of Mφs persisted up to 43 dpi and were linked to gut barrier breakdown.

DISCUSSION

The impact of respiratory tract SARS-CoV-2 infection on gut functions has been recognized as a catalyst for microbial translocation, which contributes to inflammation in COVID-19[55,74,75]. Thus, understanding GI immune pathology is a crucial step in the design of rational clinical and therapeutic strategies. However, the underlying immunological events responsible for the disruption of intestinal barrier integrity have received limited attention. This limitation arises from the challenge of accessing patients' intestinal biopsies for comprehensive studies. Here, we utilized a well-established NHP model of mild SARS-CoV-2 infection[49] to perform immunological analyses on freshly collected intestinal tissue samples obtained during the acute phase (up to 9 dpi) and the resolved phase (43 dpi) of the infection.

The detection of SARS-CoV2 RNA in rectal fluids and in intestinal tissues, although not providing definitive evidence of intestinal infection, indicates exposure of the GI tract to the virus. This finding aligns well with previous reports documenting persistent genomic viral RNA in the rectum of both cynomolgus and rhesus macaques[76,77]. Furthermore, abundant SARS-CoV-2 nucleocapsid protein and viral RNA were detected in both the large and small intestines of SARS-CoV-2–infected individuals[11,16,47,78], and viral RNA was frequently found in patient fecal samples[29,43]. In our cohort, SARS-CoV2 RNA was demonstrated in rectal fluids and in the small and large intestines of 2 out of 5 animals at 9 dpi. It is noteworthy that a similar percentage of positive samples was identified in a previously published study, which detected SARS-CoV-2 RNA in duodenal biopsies from COVID-19 patients around 8.2 days after symptoms onset[47].

Our findings suggest that animals exposed to SARS-CoV-2 exhibit notable alterations in the distribution of different immune cell subsets within intestinal tissues. Some of these alterations persisted or further intensified after the infection was resolved. However, the observed changes in immune cell proportions varied to some extent between the ileum and the colon, suggesting that SARS-CoV-2 influences the immune response differently along the intestinal tract. During the acute phase of infection, an increase in CD8$^+$ T cells was observed at both intestinal sites, which was transient although statistically significant in the colon, whereas in the ileum it tended to persist even during the resolved phase stage. Notably, these CD8$^+$ T cells exhibited high expression levels of HLA-DR, indicative of an activated phenotype. Similarly, mass cytometry analysis of small intestinal mucosa from patients, approximately 25 days after their last positive nasopharyngeal swab, revealed an augmentation in CD8$^+$ T cells along with CD8$^+$ CD103$^+$ tissue-resident memory T cells[46]. Another investigation reported the accumulation of antigen-experienced activated CD8$^+$ T cells within the duodenal epithelium, suggesting enhanced migration of cells to the intestinal mucosa during systemic SARS-CoV-2 infection[47]. Furthermore, we observed an accumulation of terminally differentiated and activated CD4$^+$ T cells, CD8$^+$ T cells, and accompanying memory B cells within the GI tract of RI animals, suggesting a robust immune response against the viral infection following respiratory exposure to SARS-CoV-2. The determination of whether these cells represent virus-specific CD4$^+$ and CD8$^+$ T cells requires further investigation. In a similar manner to recent findings in SARS-CoV-2 infected macaques' adipose tissue[79], we observed a decrease in the proportion of CD69$^+$ T cells, particularly affecting iliac CD4$^+$ T cells. CD69 is expressed on activated T cells and tissue-resident T cells and plays a crucial role in retaining T cells within tissues by inhibiting their migration[52,80–82]. The loss of CD69 expression on T cells could therefore signify significant changes in their migratory potential, potentially leading to their redistribution and contributing to systemic hyperactivation. Additionally, the absence of CD69 may also lead to functional alterations in tissue-resident T cells, which could arise from inappropriate activation[83], as indicated by the increased HLA-DR expression. This dual mechanism highlights the scientific importance of understanding the dynamics and functionality of T cells within tissues through the regulation of CD69 expression.

The analysis of the myeloid intestinal compartment revealed a significant decrease in pDCs in both the ileum and the colon throughout the infection. These findings align with a previous study that demonstrated a reduction in pDCs in the duodenum of infected patients[46]. Of note, iliac pDCs were still significantly higher during the acute phase, possibly helping the development of a memory T cell response and viral clearance[84–86]. Upon viral infection or exposure to nucleic acids, pDCs produce type I interferons (IFNs), a class of signaling proteins that assume a pivotal role in antiviral immunity while also exerting regulatory effects on immune responses in diverse ways. These interferons can inhibit the proliferation, activation, and function of T cells and memory B cells, serving as a regulatory mechanism to prevent excessive immune responses and maintain immune homeostasis[87]. The observed negative associations of pDCs with T cell activation and memory B cells could be attributed to the immunoregulative properties of pDCs, primarily mediated through the production of type I IFNs. pDCs also have the ability to interact and activate T regulatory cells through IDO expression[88,89] therefore, depletion of this specific subset in the gut compartment could lead to downregulation of Treg function and to higher T and B cell functions. Further studies are needed to elucidate those mechanisms. The colon of infected macaques was also affected by a significative reduction of CD4$^+$ T cells, DCs, and Mφs. These alterations in the immune system may contribute to the breakdown of the intestinal epithelial barrier and could also explain the GI symptoms observed in patients after

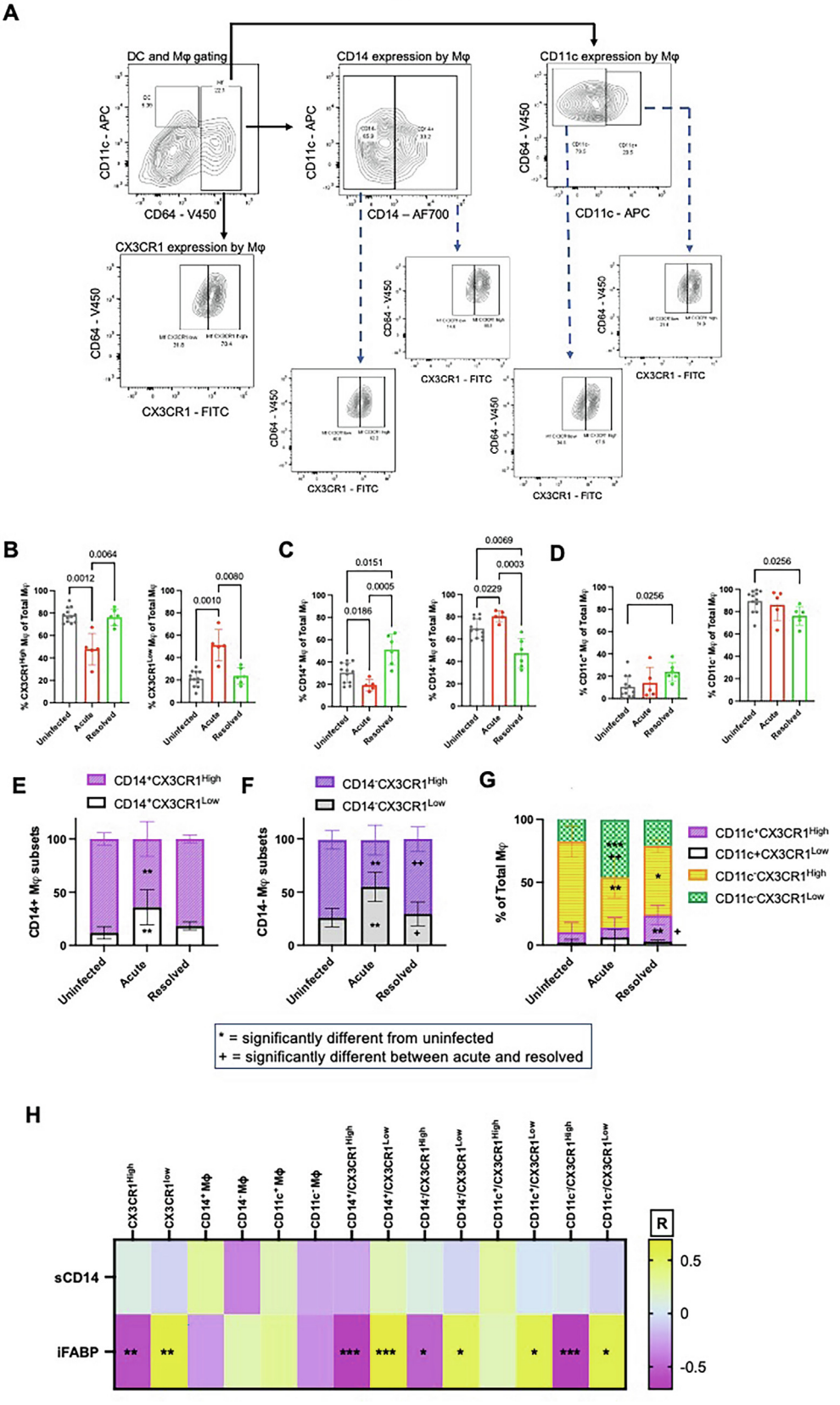
A
DC and Mφ gating
CD14 expression by Mφ
CD11c expression by Mφ
CD11c - APC
CD64 - V450
CD14 – AF700
CX3CR1 expression by Mφ
CX3CR1 - FITC
B
C
D
Uninfected
Acute
Resolved
E
CD14+CX3CR1High
CD14+CX3CR1Low
CD14+ Mφ subsets
F
CD14-CX3CR1High
CD14-CX3CR1Low
CD14- Mφ subsets
G
CD11c+CX3CR1High
CD11c+CX3CR1Low
CD11c-CX3CR1High
CD11c-CX3CR1Low
% of Total Mφ
* = significantly different from uninfected
+ = significantly different between acute and resolved
H
CX3CR1High
CX3CR1low
CD14+Mφ
CD14-Mφ
CD11c+Mφ
CD11c-Mφ
CD14+/CX3CR1High
CD14+/CX3CR1Low
CD14-/CX3CR1High
CD14-/CX3CR1Low
CD11c+/CX3CR1High
CD11c+/CX3CR1Low
CD11c-/CX3CR1High
CD11c-/CX3CR1Low
sCD14
iFABP
R
0.5
0
-0.5

the resolution of SARS-CoV-2 infection[35]. Our results are consistent with a previous study that showed a decrease in conventional DCs in individuals with COVID-19 using CyTOF and transcriptional approaches[46]. To the best of our knowledge, the analysis of intestinal T lymphocyte subsets in COVID patients has not been conducted. It's tempting to speculate that the observed decline in $CD4^+$ T cells during the resolved phase of infection may be accompanied by a reduction of Th17 and/or Th22 cells, two subsets of T-helper cells known to play crucial roles in maintaining the integrity and functionality of the intestinal mucosal barrier[90,91]. Further studies are needed to assess whether dysregulation of the Th17 and Th22 cell leading to intestinal barrier dysfunction occurs as a consequence of systemic SARS-CoV-2 infection, as previously shown with HIV/SIV infection[92–94] and various inflammatory and autoimmune diseases, such as inflammatory bowel disease (IBD).

The reduction of colonic Mφs we observed in SARS-CoV-2 exposed macaques was paralleled by changes in the composition of specific Mφ subsets and in the expression patterns of CX3CR1. Within the intestinal lamina propria, two major subsets of Mφs can be identified based on their CX3CR1 expression levels: $CX3CR1^{High}$ Mφs constitute the predominant population during homeostasis[67,71,95,96], whereas the $CX3CR1^{Low}$ Mφs subset expands in response to inflammatory stimuli[67,71,97,98]. In uninfected animals, we found that approximately 80% of colonic Mφs expressed high levels of CX3CR1 ($CX3CR1^{High}$), and relatively low levels of CD11c and CD14, a phenotype typical of resident cells similar to what described in human and mice studies[67,96,99,100]. $CX3CR1^{High}$ Mφs were repeatedly described as anti-inflammatory cells characterized by high expression of scavenger receptors, and low production of pro-inflammatory cytokines[67,71,95,96]. These Mφs actively contribute to the maintenance of intestinal epithelial barrier integrity and tolerance by promoting tissue repair, phagocytosing apoptotic cells, and inducing the differentiation of regulatory T cells[101–104]. In contrast, during inflammation and infection events, such as IBD[105] and early HIV/SIV infection[72], lamina propria Mφs undergo dynamic changes in their phenotype and function. They can adopt a pro-inflammatory phenotype characterized by reduced expression of CX3CR1, increased expression of MHC-II and co-stimulatory molecules, and pro-inflammatory cytokines, thus contributing to the breakdown of the intestinal barrier[21,67,71,97,98]. In line with these observations, during the acute phase of SARS-CoV-2 infection, $CX3CR1^{High}$ Mφs were significantly reduced whereas $CX3CR1^{Low}$ cells expanded. The accumulation of $CX3CR1^{Low}$ Mφs correlated with the increase of iFABP, indicating that these cells directly contributed to intestinal epithelial damage. Of note, after the resolution of systemic infection, not only colonic Mφs were greatly reduced in AI animals but also displayed a phenotype only partially resembling that of uninfected controls, characterized by similar levels of CX3CR1 but significantly higher expression of both CD11c and CD14, indicating recent gut recruitment. A similar phenotype was described for intestinal Mφs of COVID-19 patients[47]. $CD14^+$ mononuclear phagocytes were shown to accumulate in the inflamed gut in settings such as IBD[106], arising from circulating precursors[107]. Therefore, our results suggest perturbation of the intestinal Mφ homeostasis after the clearance of the virus, which could potentially have long-term consequences. Furthermore, $CX3CR1^+$ Mφs are an essential target of regulation by the microbiota[108–110], and intestinal dysbiosis was observed in both SARS-CoV-2 infected patients[111] and NHPs[112], thereby supporting the hypothesis that compromised intestinal barriers may facilitate bacterial translocation and contribute to post-acute sequelae associated with SARS-CoV-2 infection.

Our study presents compelling evidence indicating that respiratory tract SARS-CoV-2 infection in macaques triggers an inflammatory response in the GI tract, possibly resulting in microbial translocation. This phenomenon was evidenced by increased levels of FC and sCD14 during the resolved infection phase when the virus was undetectable in both the respiratory and the intestinal tracts. In contrast, the acute infection phase was characterized by elevated levels of iFABP, suggesting that initial damage to enterocytes, measurable during active viral replication, translates into enhanced gut permeability and localized inflammation, which remains detectable at 43 dpi. Our findings align with previous studies in humans that showed increased levels of sCD14 in infected patients[39] and identified iFABP as a biomarker for assessing the severity of COVID-19 upon admission[39,113]. The observed elevation in sCD14 level, despite the concurrent reduction in colonic Mφs numbers, can be related to the significant frequency of $CD14^+$ Mφs observed in RI animals. A positive, although not statistically significant correlation was indeed observed between sCD14 and $CD14^+$ Mφs. This phenomenon underscores the intricate interplay between diverse Mφs subsets and their unique functional roles. Furthermore, it is worth noting that, in addition to $CD14^+$ Mφs and activated monocytes, neutrophils could also serve as potential sources of sCD14[114]. Additionally, FC has emerged as a reliable indicator of intestinal inflammation in COVID-19 cases, and con-

Fig. 5 Changes in the proportion of colonic macrophage subsets over the course of SARS-CoV-2 infection and their association with markers of intestinal barrier disruption. (A) $CD64^+$ colonic macrophages (Mφs) were analyzed by flow cytometry for the expression of CX3CR1, CD14, and CD11c receptors (black arrows). Levels of CX3CR1 expression were further evaluated on subsets of $CD14^+$ and $CD14^-$ Mφ, and of $CD11c^+$ and $CD11c^-$ Mφ (blue dashed arrows). An uninfected control animal is shown as an example. Mφs subsets from AI (n = 5) and RI (n = 6) SARS infection groups along with 12 uninfected controls are represented as the frequency of the parental Mφ population: (B) $CX3CR1^{High}$ and $CX3CR1^{Low}$ Mφs, (C) $CD14^+$ and $CD14^-$ Mφs, (D) $CD11c^+$ (immature) and $CD11c^-$ (mature) Mφs. (E) Proportion of $CD14^+$ $CX3CR1^{High}$ and $CD14^+$ $CX3CR1^{Low}$ Mφs in uninfected, AI, and RI animals. (F) Proportion of $CD14^-$ $CX3CR1^{High}$ and $CD14^-$ $CX3CR1^{Low}$ Mφs in uninfected, AI, and RI animals. (G) Proportion of $CD11c^+$ $CX3CR1^{High}$, $CD11c^+$ $CX3CR1^{Low}$, $CD11c^-$ $CX3CR1^{High}$, and $CD11c^-$ $CX3CR1^{Low}$ Mφs in uninfected, AI, and RI animals. (H) Heatmap representation of Spearman xy correlation analysis between the proportion of colonic macrophage subsets (among total macrophages) in uninfected, AI, and RI animals with sCD14 and iFABP. The obtained correlation factors (R) are shown on the heatmap with a yellow (positive correlation) to pink (negative correlation) scale. Significant p values are indicated as follows: $*p \leq 0.05$, $**p \leq 0.01$, $***p \leq 0.001$, $****p \leq 0.0001$.

sistent with our observations, FC levels did not correlate with fecal SARS-CoV-2 RNA in a prior human study[43]. However, within our cohort, we identified a positive correlation between FC and sCD14 levels, thereby providing support for the concept that immune activation and intestinal inflammation are interlinked. In addition, our results suggest that immature neutrophils in the colon of animals from the resolved phase are a potential source of FC, aligning with a study that investigated blood and lung samples from COVID-19 patients and revealed an increase in immature neutrophils and FC in individuals with mild symptoms[115]. These observations hold significance in the context of intestinal inflammatory conditions affecting individuals infected with SARS-CoV-2, as the inflammatory response observed in the gut has the potential to worsen the course of human IBD.

We acknowledge some limitations of our study. Firstly, our investigation focused on immunological data obtained from animals exposed to the original Wuhan strain of SARS-CoV-2. This implies that the impact on intestinal immunity caused by other variants, such as Delta or Omicron, might vary, requiring further research. In an intestinal organoid model, it was observed that the Delta variant had a higher ability to infect intestinal cells compared to the Wuhan and Omicron strains[116]. This discrepancy in infectivity and replication could potentially affect the development of GI symptoms. Notably, individuals infected with the Delta variant showed a higher incidence of GI disorders compared to those infected with the Wuhan and Omicron variants[117,118]. However, more investigations are needed to determine if these differences in infectivity and GI symptoms are associated with distinct alterations in the intestinal immune system. Additionally, 2 out of 6 RI animals were exposed to a 10-fold lower viral infectious dose. Although we did not detect any difference in the AUC of viral load during the first 9 days of infection, the infectious dose needs to be carefully considered when evaluating the kinetics of viral replication and other immunological features in NHP models. Secondly, unlike hospitalized human patients, the study utilized young animals that did not exhibit acute lung inflammation. This discrepancy limits the ability to generalize the findings to severe respiratory cases in humans. Thirdly, the study included a limited number of animals, and not all negative control samples had available ileum specimens. As a result, the analysis of immune cell phenotyping, specifically the examination of ileum neutrophils, was performed on a limited sample size. In addition, stratification of animal subjects based on their biological sex was unfeasible in this study. Epidemiological data have documented a sexual dimorphism in the clinical presentation and severity of COVID-19[119–121]. Therefore, the undertaking of sex-specific investigations pertaining to GI barrier integrity and immune response in forthcoming studies may offer valuable insights into the relatively more favorable course of the disease in women compared to men. Lastly, the correlation analysis we performed in this study serves as a preliminary investigation, and we acknowledge the need for future research to conduct confirmatory analyses that rigorously validate the observed correlations in a more hypothesis-driven context.

In conclusion, our study elucidates crucial immune mechanisms involved in the intestinal host response to SARS-CoV-2, thereby enhancing our comprehension of the disease's pathogenesis. Our findings suggest that the perturbation of intestinal macrophage homeostasis plays a role in the impairment of gut functions, the breakdown of the intestinal epithelial barrier, and potentially in the development of long-term clinical complications. Consequently, interventions aimed at targeting the gut, and preventing gut barrier defects, hold promise as potential strategies to enhance outcomes in patients with COVID-19.

METHODS

Ethics and biosafety statement

Cynomolgus (C.) macaques (*Macaca fascicularis*) originating from Mauritian AAALAC-certified breeding centers were housed in IDMIT facilities (CEA, Fontenay-aux-Roses), under BSL-2 and BSL-3 containment when necessary (Animal facility authorization #D92032-02, Prefecture des Hauts de Seine, France) and in compliance with European Directive 2010/63/EU, the French regulations and the Standards for Human Care and Use of Laboratory Animals, of the Office for Laboratory Animal Welfare (OLAW, assurance number #A5826-01, US). The protocols were approved by the institutional ethical committee "Comité d'Ethique en Expérimentation Animale du Commissariat à l'Energie Atomique et aux Energies Alternatives" (CEtEA #44) under statement number A20_011. These studies were authorized by the "Research, Innovation, and Education Ministry" under registration numbers APAFIS#24434-2020030216532863 v1.

Study design and clinical follow-up

Thirty C. macaques aged 40 – 126 months (14 females and 16 males, Table S1) were included in this study of which 11 macaques (9 males and 2 females) were exposed to SARS-CoV-2 virus and 19 were negative controls. Among the SARS-CoV-2 infected animals, 5 were euthanized at 7 to 9 days post-infection (dpi) and assigned to the "acute infection group", whereas the remaining were examined at 43 dpi and assigned to the "resolved infection group". The study design and sample collection are shown in Fig. 1A.

Animals were followed daily and any abnormal behavior was reported in a specific individual file. Clinical measurements including body weight and rectal temperature were recorded at baseline and daily up to 7 to 12 dpi. Blood was available at baseline and euthanasia from both infection groups and daily during the follow-up from the acute infection group (Fig. 1A). Tracheal and nasopharyngeal swabs were collected between 0 and 9 dpi from both infected groups whereas rectal swabs were collected from the acute infection group at baseline, 2 dpi, 5 dpi, and at euthanasia, and from resolved infection group at euthanasia. Blood cell counts, hemoglobin, and hematocrit were determined from EDTA blood using a DXH800 analyzer (Beckman Coulter, USA). Sample collection at necropsies included blood and fluids, stool, ileum, descending/sigmoid colon, and rectum from both infected groups, plus the lung from the acute infected group. The same type of sample was collected, when available, from uninfected negative control animals (Table S2). Tissues were either stored for viral load quantification (ileum, descending/sigmoid colon, rectum, and lung) or used for immune cell phenotyping (ileum and descending/sigmoid colon).

Infection of macaques

Cynomolgus macaques were exposed to either 1×10^6 plaque-forming unit (pfu) (n = 9) or 1×10^5 pfu (n = 2; Table S2) of SARS-CoV-2 virus (BetaCoV/France/IDF/0372/2020 strain, provided by the National Reference Center for Respiratory Viruses (Institut Pasteur, France) through a combination of intranasal and intratracheal routes, as previously described[122]. Animals were

premedicated with atropine (0.04 mg/kg) intramuscularly and then sedated with medetomidine (domitor 0.03 mg/kg and ketamine 1000 at 10 mg/kg also given intramuscularly). Using a laryngoscope, animals were intubated with the nasogastric tube (size 2.6 mm diameter/40 cm COVETO) and the endotracheal tube (size 3 mm diameter/16 cm COVETO), at a 1 cm distance. Animals were inoculated under class II biological safety cabinet, in a supine recumbency position. For the intranasal challenge, the viral inoculum of 250 µL was applied into each nostril and massaged in using a 1 mL micropipette, after which a 5mL syringe was introduced into the endotracheal tube to apply 4.5 mL of the viral inoculum to the trachea. To ensure the inoculation of the viral preparation, a 2 mL volume of air was injected into the nasogastric tube. Finally, the animal's face was wiped clean of any residual virus.

Virus quantification

Viral RNA loads were assessed in tracheal, nasopharyngeal, and rectal swabs collected in Viral Transport Medium (VTM, CDC, DSR052-01), and stored at 2 to 8 °C until examined by RT-qPCR. Fragments of 50 mg of tissues collected at euthanasia including the ileum, colon, and rectum from both infection groups and the lung only from the acute infection group, were lysed in NucleoZOL (Machery-Nagel, Duren, Germany) using a Precellys device (Bertin Technology, Montigny-le-Bretonneux, France). RNA was isolated from swabs and tissues, using respectively the NucleoSpin Virus Core Kit (Macherey-Nagel) and the NucleoSpin RNA Core Kit (Macherey-Nagel). Reverse transcription and qPCR were performed according to the manufacturers' instructions using the SuperScript III Platinium One-step Quantitative RT-qPCR System (Life Technologies). A viral culture of known concentration was used as standard curve. The protocol for SARS-CoV-2 IP4 genomic mRNA (gRNA) measure is as detailed in the WHO protocol for SARS detection[123], with an estimated limit of detection (LOD) of 4.76×10^2 copies of SARS-CoV-2 gRNA per mL and an estimated limit of quantification (LOQ) of 4.76×10^3 copies/mL. SARS-CoV-2 E gene sub-genomic mRNA (sgRNA) levels were assessed by RT-qPCR using primers and probes previously described[124], and LOD and LOQ were 4.31×10^2 and 4.31×10^3 copies/mL, respectively.

Validation cohort to assess the duration of viral load detection in fluids

Genomic RNA levels were assessed in tracheal, nasopharyngeal and rectal fluids collected at 0, 2, 5, 7, 9, 13, 16, 20 and 27 dpi from 32 macaques exposed to 1×10^6 pfu of SARS-CoV-2 virus (BetaCoV/France/IDF/0372/2020 strain). 28 animals were historical controls used in previously published studies[49,122,125,126] whereas data from 4 macaques are unpublished. Results are shown in Supplementary Fig. 1F.

Soluble factors quantification

Serum concentrations of soluble CD14 (sCD14) and intestinal Fatty Acid Binding Protein (iFABP) from SARS-CoV-2 exposed animals and from 9 negative controls were quantified using the human CD14 ELISA kit (R&D Systems, UK) and the monkey iFABP ELISA kit (Clinisciences, USBiologicals, USA), respectively, according to manufacturer's instructions. Plates were read using a TECAN SPARK 10M reader. Fractalkine concentration in serum was estimated using the U-PLEX NHP Fractalkine Assay from MesoScale Discovery and a MESO QuickPlex SQ 120 reader (MSD, USA) according to the manufacturer's instructions. Calprotectin level was evaluated in stools from SARS-CoV-2 exposed animals and 6 negative controls using the CALPROLAB Calprotectin ELISA (ALP) kit (Calpro, Norway) according to the manufacturer's instructions.

Tissue processing and lamina propria mononuclear cells isolation and phenotyping

Colon and ileum were collected at animal's necropsy from 15 or 8 uninfected control animals respectively (Table S2), in addition to all the SARS-CoV-2 exposed animals, and were immediately processed to isolate lamina propria mononuclear cells (LPMCs), as previously described[68,72]. Tissues were cut into small pieces and incubated for 20 min at 37°C in HBSS medium without Ca^{++}/Mg^{++} (Fisher Scientific, Illkirch, France) supplemented with 5 mM EDTA and 1 mM DTT (Sigma-Aldrich, St Quantin Fallavier, France) to eliminate mucus and epithelial cells. After washing in PBS, the tissue was incubated for 1 h at 37°C with agitation in HBSS medium with Ca^{++}/Mg^{++} (Fisher Scientific, Illkirch, France) containing collagenase type VIII (0.25 mg/ml, Sigma Aldrich, St Quantin Fallavier, France) and DNase (5 U/ml, Roche, Mannheim, Germany). Undigested pieces were submitted to second digestion for 30 min. Cell suspensions from ileum and colon were filtered through 70-mm sterile nylon cell strainers (BD Biosciences), washed with complete medium (RPMI supplemented with 10% FCS, 100 U/ml penicillin/streptomycin, 1% glutamine, 1% NEAA, 1% Na-pyruvate, 1% HEPES buffer [1 M.; all from Fisher Scientific, Illkirch, France) and analyzed by flow cytometry. Three antibody panels (Myeloid for pDCs, mDCs, and macrophages; Lymphoid for $CD4^+$ and $CD8^+$ T lymphocytes, and B lymphocytes; and Neutrophil) were established (Table S3). When a limited number of cells was available, priority was given to the myeloid panel (Table S2). Cells were acquired on an LSR Fortessa (BD Biosciences) and results were analyzed using FlowJo 9.8.3 (Tristar, USA) software within the singlet viable fraction. Positive and negative gating was set using the fluorescence minus one (FMO) method.

Quantification and statistical analysis

All data visualization and statistical analyses were carried out using Prism v9.2.0 software (GraphPad Software, La Jolla, USA). The differences in cellular populations and soluble factors between the three experimental groups were assessed using the One-Way ANOVA and nonparametric test (Kruskal-Wallis test) and p values were corrected for multiple comparisons using the Benjamini, Krieger and Yekutieli FDR approach. The exact q-value (i.e. p-value corrected for multiple comparisons) is shown in each figure.

For correlations between viral load in intestinal tissues and rectal fluids, a multiple variable table was used to generate a non-parametric Spearman correlation matrix and finally represented as a double gradient color map. For all the other correlation analyses, a non-parametric XY Spearman test was performed and represented as heat maps based on the obtained R correlation factors. The significance is depicted as one or more (*) shown on the correlation matrix or heatmaps according to the p-value. p-value ≤ 0.05 was considered significant and represented in the following manner: $*p \leq 0.05$, $**p \leq 0.01$, $***p \leq 0.001$, $****p \leq 0.0001$.

Analysis was performed at the specified time points and including the experimental groups as indicated in the figure legends.

AUTHOR CONTRIBUTIONS

Study conception and design: MC and SH. Acquisition of the data: SH, KB, RM, and LB. Analysis and interpretation of the data: SH, KL, RM, NDB, MC. Animal handling: SL and FR. Ethical documentation: NDB. Draft of the manuscript: MC. Tables and figures preparation: KL, SH, and MC. Funding acquisition: RLG and MC. All authors read, corrected, and approved the final version of the manuscript. Equal author contribution was listed in alphabetical order.

DECLARATION OF COMPETING INTERESTS

The authors have no competing interests to declare.

FUNDING

This work was supported by the "Programme Investissements d'Avenir" (PIA) managed by the ANR under reference ANR-11-INBS-0008, funding the Infectious Disease Models and Innovative Therapies (IDMIT, Fontenay-aux-Roses, France) infrastructure, and ANR-10-EQPX-02-01, funding the FlowCyTech facility (IDMIT, Fontenay-aux-Roses, France). The project was also supported by the ANRS-MIE (France), the REACTing action, and the Fondation pour la Recherche Médicale (FRM, France, AM-CoV-Path project). The funders had no role in the design of the study, data collection or interpretation, or the decision to submit the work for publication.

DATA AVAILABILITY

All data needed to evaluate the conclusions of the paper are present in the manuscript or the Supplementary Information.

ACKNOWLEDGMENTS

We are grateful for the excellent contributions of the veterinarians and of the staff at the IDMIT center. We thank Quentin Sconosciuti, Nina Dhooge, Maxime Potier, Quentin Pascal, Benoit Delache, Julien Lemaitre, Victor Magneron, Claire-Maelle Fovet, Johana Demilly, Pauline Le Calvez, Jean-Marie Robert, Thierry Prot and Cristina Dodan for the NHP experiments; P. Maisonnasse for project management; M. Galpin-Lebreau, Loïc Pintore, Laurine Moenne-Loccoz, L. Junges, and K. Lheureux for the RT-qPCR experiments; Julien Dinh, Mylinda Barendji and Elodie Guyon for the management of NHP biological resources; Cécile Herate for providing viral loads data from historical control animals; F. Ducancel, Y. Gorin, B. Targat, S. Keser and I. Mangeot for their help with the logistics, safety, and resource management and all members of the FlowCyTech, ASW, LIBI, L2I, and L3I core facilities. We thank Sylvie van Der Werf at the National Reference Centre for Respiratory Viruses (Institut Pasteur) for providing the SARS-CoV-2 virus.

APPENDIX A. SUPPLEMENTARY DATA

Supplementary data to this article can be found online at https://doi.org/10.1016/j.mucimm.2023.10.001.

References

1. World Health Organization. SARS report. Available at: https://www.who.int/health-topics/severe-acute-respiratory-syndrome#tab=tab_1
2. Cai, J. et al. Indirect virus transmission in cluster of COVID-19 cases, Wenzhou, China, 2020. *Emerg. Infect. Dis.* **26**, 1343–1345 (2020).
3. Bae, S. et al. Epidemiological characteristics of COVID-19 outbreak at Fitness Centers in Cheonan, Korea. *J. Korean Med. Sci.* **35**, e288 (2020).
4. Guan, W. J. et al. Clinical characteristics of coronavirus disease 2019 in China. *N. Engl. J. Med.* **382**, 1708–1720 (2020).
5. He, X. et al. Temporal dynamics in viral shedding and transmissibility of COVID-19. *Nat. Med.* **26**, 672–675 (2020).
6. Huang, C. et al. Clinical features of patients infected with 2019 novel coronavirus in Wuhan, China. *Lancet.* **395**, 497–506 (2020).
7. Chen, G. et al. Clinical and immunological features of severe and moderate coronavirus disease 2019. *J. Clin. Invest.* **130**, 2620–2629 (2020).
8. Blanco-Melo, D. et al. Imbalanced Host Response to SARS-CoV-2 Drives Development of COVID-19. *Cell.* **181**, 1036–1045.e9 (2020).
9. Chi, Y. et al. Serum cytokine and chemokine profile in relation to the severity of coronavirus disease 2019 in China. *J. Infect. Dis.* **222**, 746–754 (2020).
10. Zhou, Z. et al. Heightened innate immune responses in the respiratory tract of COVID-19 patients. *Lcell host Microbe.* **27**, 883–890 (2020).
11. Xiao, F. et al. Evidence for gastrointestinal infection of SARS-CoV-2. *Gastroenterology* **158**, 1831–1833.e3 (2020).
12. Escher, F. et al. Detection of viral SARS-CoV-2 genomes and histopathological changes in endomyocardial biopsies. *ESC Heart Fail.* **7**, 2440–2447 (2020).
13. Braun, F. et al. SARS-CoV-2 renal tropism associates with acute kidney injury. *Lancet* **396**, 597–598 (2020).
14. Dickson, R. P. et al. Enrichment of the lung microbiome with gut bacteria in sepsis and the acute respiratory distress syndrome. *Nat. Microbiol.* **1**, 16113 (2016).
15. Dumas, A., Bernard, L. & Neyrolles, O. The role of the lung microbiota and the gut–lung axis in respiratory infectious diseases. *Cell. Microbiol.* **20**, 1–9 (2018).
16. Qian, Q. et al. Direct evidence of active SARS-CoV-2 replication in the intestine. *Clin. Infect. Dis.* **73**, 361–366 (2021).
17. Jiao, L. et al. The gastrointestinal tract is an alternative route for SARS-CoV-2 infection in a nonhuman primate model. *Gastroenterology* **160**, 1647–1661 (2021).
18. Zang, R. et al. TMPRSS2 and TMPRSS4 promote SARS-CoV-2 infection of human small intestinal enterocytes. *Sci. Immunol.* **5**, 1–14 (2020).
19. Lamers, M. M. et al. SARS-CoV-2 productively infects human gut enterocytes. *Science* **369**, 50–54 (2020).
20. Wyler, E. et al. Transcriptomic profiling of SARS-CoV-2 infected human cell lines identifies HSP90 as target for COVID-19 therapy. *iScience* **24**:102151.
21. Ravindra, N. G. et al. Single-cell longitudinal analysis of SARS-CoV-2 infection in human airway epithelium identifies target cells, alterations in gene expression, and cell state changes. *PLOS Biol.* **19**, e3001143 (2021).
22. Triana, S. et al. Single-cell analyses reveal SARS-CoV-2 interference with intrinsic immune response in the human gut. *Mol. Syst. Biol.* **17**, e10232 (2021).
23. Guery, B. et al. Clinical features and viral diagnosis of two cases of infection with Middle East Respiratory Syndrome coronavirus: a report of nosocomial transmission. *Lancet* **381**, 2265–2272 (2013).
24. Chan, P. K. S. et al. Laboratory diagnosis of SARS. *Emerg. Infect. Dis.* **10**, 825–831 (2004).
25. Cheng, P. K. C. et al. Viral shedding patterns of coronavirus in patients with probable severe acute respiratory syndrome. *Lancet* **363**, 1699–1700 (2004).
26. Chan, M. C. W., Lee, N., Chan, P. K. S., Leung, T. F. & Sung, J. J. Y. Fecal detection of influenza A virus in patients with concurrent respiratory and gastrointestinal symptoms. *J. Clin. Virol.* **45**, 208–211 (2009).
27. Arena, C. et al. Simultaneous investigation of influenza and enteric viruses in the stools of adult patients consulting in general practice for acute diarrhea. *Virol. J.* **9**, 116 (2012).
28. Wu, Y. et al. Prolonged presence of SARS-CoV-2 viral RNA in faecal samples. *Lancet Gastroenterol. Hepatol.* **5**, 434–435 (2020).
29. Cheung, K. S. et al. Gastrointestinal manifestations of SARS-CoV-2 infection and virus load in fecal samples from a Hong Kong cohort : systematic review and meta-analysis. *Gastroenterology* **159**, 81–95 (2020).
30. Hashem, W. M., Abdelaziz, H., Sallam, D. E., Ismail, M. A. & Ahmed, A. E. Impact of COVID-19 on digestive system: prevalence, clinical characteristics, outcome, and relation to the severity of COVID-19. *Egypt. J. Intern. Med.* **34**, 45 (2022).
31. Leung, W. K., To, K. F. & Chan, P. K. S. Enteric Involvement of severe acute respiratory syndrome – associated coronavirus infection. *Gastroenterology* **5085**, 1011–1017 (2003).
32. Jin, X. et al. Epidemiological, clinical and virological characteristics of 74 cases of coronavirus-infected disease (COVID-19) with gastrointestinal symptoms. *Gut* **69**, 1002–1009 (2020).
33. Menon, T. et al. Association of gastrointestinal system with severity and mortality of COVID-19: a systematic review and meta-analysis. *Cureus* **13**, e13317 (2021).
34. Shah, S. C. et al. Associations between gastrointestinal symptoms and COVID-19 severity outcomes based on a propensity score–weighted analysis of a nationwide cohort. *Gastro Hep. Adv.* **1**, 977–984 (2022).
35. Noviello, D. et al. Functional gastrointestinal and somatoform symptoms five months after SARS-CoV-2 infection: a controlled cohort study. *Neurogastroenterol. Motil.* **34**, e14187 (2022).

36. Xu, E., Xie, Y. & Al-Aly, Z. Long-term gastrointestinal outcomes of COVID-19. *Nat. Commun.* **14**, 983 (2023).
37. Mao, R. et al. Manifestations and prognosis of gastrointestinal and liver involvement in patients with COVID-19: a systematic review and meta-analysis. *Lancet Gastroenterol. Hepatol.* **5**, 667–678 (2020).
38. Assiri, A. et al. Epidemiological, demographic, and clinical characteristics of 47 cases of Middle East respiratory syndrome coronavirus disease from Saudi Arabia: a descriptive study. *Lancet Infect. Dis.* **13**, 752–761 (2013).
39. Giron, L. B. et al. Plasma markers of disrupted gut permeability in severe COVID-19 patients. *Front. Immunol.* **12**:686240.
40. Tyszko, M. et al. Intestinal fatty acid binding protein (I-FABP) as a prognostic marker in critically ill COVID-19 patients. *Pathogens* **11**, 1–15 (2022).
41. Golonka, R. M. et al. Harnessing innate immunity to eliminate SARS-CoV-2 and ameliorate COVID-19 disease. *Physiol. Genomics* **52**, 217–221 (2020).
42. Ye, Q., Wang, B., Zhang, T., Xu, J. & Shang, S. The mechanism and treatment of gastrointestinal symptoms in patients with COVID-19. *Am. J. Physiol. Gastrointest. Liver Physiol.* **319**, G245–G252 (2020).
43. Effenberger, M. et al. Faecal calprotectin indicates intestinal inflammation in COVID-19. *Gut* **69**, 1543–1544 (2020).
44. Adriana, D. N. et al. Role of fecal calprotectin as a hypoxic intestinal damage biomarker in COVID-19 patients. *Gut Pathog.* **14**, 34 (2022).
45. Wang, C. et al. Imaging mass cytometric analysis of postmortem tissues reveals dysregulated immune cell and cytokine responses in multiple organs of COVID-19 patients. *Front. Microbiol.* **11**:600989.
46. Livanos, A. E. et al. Intestinal Host Response to SARS-CoV-2 Infection and COVID-19 Outcomes in Patients With Gastrointestinal Symptoms. *Gastroenterology* **160**, 2435–2450.e34 (2021).
47. Lehmann, M. et al. Human small intestinal infection by SARS-CoV-2 is characterized by a mucosal infiltration with activated CD8+ T cells. *Mucosal Immunol.* **14**, 1381–1392 (2021).
48. Arunachalam, P. S. et al. Systems biological assessment of immunity to mild versus severe COVID-19 infection in humans. *Science* **369**, 1210–1220 (2020).
49. Maisonnasse, P. et al. Hydroxychloroquine use against SARS-CoV-2 infection in non-human primates. *Nature* **585**, 584–587 (2020).
50. Fahlberg, M. D. et al. Cellular events of acute, resolving or progressive COVID-19 in SARS-CoV-2 infected non-human primates. *Nat. Commun.* **11**, 6078 (2020).
51. Imamichi, H. et al. The CD8+HLA-DR+ T cells expanded in HIV-1 infection are qualitatively identical to those from healthy controls. *Eur. J. Immunol.* **42**, 2608–2620 (2012).
52. Wang, X. et al. Distinct expression patterns of CD69 in mucosal and systemic lymphoid tissues in primary SIV infection of rhesus macaques. *PLoS One* **6**, e27207 (2011).
53. Veazey, R. S. et al. Identifying the target cell in primary simian immunodeficiency virus (SIV) infection: highly activated memory CD4 + T cells are rapidly eliminated in early SIV infection in vivo. *J. Virol.* **74**, 57–64 (2000).
54. Henson, S. M., Riddell, N. E. & Akbar, A. N. Properties of end-stage human T cells defined by CD45RA re-expression. *Curr. Opin. Immunol.* **24**, 476–481 (2012).
55. Eleftheriotis, G. et al. Alterations in gut immunological barrier in SARS-CoV-2 infection and their prognostic potential. *Front. Immunol.* **14**, 1129190 (2023).
56. Wu, X. et al. Intestinal damage in COVID-19: SARS-CoV-2 infection and intestinal thrombosis. *Front. Microbiol.* **13**:860931.
57. Yamada, S. et al. SARS-CoV-2 induces barrier damage and inflammatory responses in the human iPSC-derived intestinal epithelium. *J. Pharmacol. Sci.* **149**, 139–146 (2022).
58. Hoffmanová, I. et al. Serological markers of enterocyte damage and apoptosis in patients with celiac disease, autoimmune diabetes mellitus and diabetes mellitus type 2. *Physiol. Res.* **64**, 537–546 (2015).
59. Adriaanse, M. P. M. et al. Serum I-FABP as marker for enterocyte damage in coeliac disease and its relation to villous atrophy and circulating autoantibodies. *Aliment. Pharmacol. Ther.* **37**, 482–490 (2013).
60. Derikx, J. P. M. et al. A pilot study on the noninvasive evaluation of intestinal damage in celiac disease using I-FABP and L-FABP. *J. Clin. Gastroenterol.* **43**, 727–733 (2009).
61. Konikoff, M. R. & Denson, L. A. Role of fecal calprotectin as a biomarker of intestinal inflammation in inflammatory bowel disease. *Inflamm. Bowel Dis.* **12**, 524–534 (2006).
62. Bjarnason, I. The use of fecal calprotectin in inflammatory bowel disease. *Gastroenterol. Hepatol. (N Y)* **13**, 53–56 (2017).
63. Pathirana, W. G. W., Chubb, S. P., Gillett, M. J. & Vasikaran, S. D. Faecal calprotectin. *Clin. Biochem. Rev.* **39**, 77–90 (2018).
64. Jukic, A., Bakiri, L., Wagner, E. F., Tilg, H. & Adolph, T. E. Calprotectin: from biomarker to biological function. *Gut* **70**, 1978–1988 (2021).
65. Yip, J. L. K., Balasuriya, G. K., Spencer, S. J. & Hill-Yardin, E. L. The role of intestinal macrophages in gastrointestinal homeostasis: heterogeneity and implications in disease. *Cell. Mol. Gastroenterol. Hepatol.* **12**, 1701–1718 (2021).
66. Han, X., Ding, S., Jiang, H. & Liu, G. Roles of macrophages in the development and treatment of gut inflammation. *Front. Cell Dev. Biol.* **9**:625423.
67. Bain, C. C. & Mowat, A. M. Macrophages in intestinal homeostasis and inflammation. *Immunol. Rev.* **260**, 102–117 (2014).
68. Benmeziane, K. et al. Isolation and phenotypic characterization of human and nonhuman primate intestinal lamina propria mononuclear cells. *Star Protoc.* **3**:101815.
69. Smith, P. D. et al. Intestinal macrophages lack CD14 and CD89 and consequently are down-regulated for LPS- and IgA-mediated activities. *J. Immunol.* **167**, 2651–2656 (2001).
70. Medina-Contreras, O. et al. CX3CR1 regulates intestinal macrophage homeostasis, bacterial translocation, and colitogenic Th17 responses in mice. *J. Clin. Invest.* **121**, 4787–4795 (2011).
71. Weber, B., Saurer, L., Schenk, M., Dickgreber, N. & Mueller, C. CX3CR1 defines functionally distinct intestinal mononuclear phagocyte subsets which maintain their respective functions during homeostatic and inflammatory conditions. *Eur. J. Immunol.* **41**, 773–779 (2011).
72. Cavarelli, M. et al. Identification of CX3CR1+ mononuclear phagocyte subsets involved in HIV-1 and SIV colorectal transmission. *iScience* **25**:104346.
73. Umehara, H. et al. Fractalkine in vascular biology: from basic research to clinical disease. *Arterioscler. Thromb. Vasc. Biol.* **24**, 34–40 (2004).
74. Trottein, F. & Sokol, H. Potential causes and consequences of gastrointestinal disorders during a SARS-CoV-2 infection. *Cell Rep.* **32**:107915.
75. Velikova, T. et al. Gastrointestinal mucosal immunity and COVID-19. *World J. Gastroenterol.* **27**, 5047–5059 (2021).
76. Munster, V. J. et al. Respiratory disease in rhesus macaques inoculated with SARS-CoV-2. *Nature* **585**, 268–272 (2020).
77. Fovet, C. M. et al. A case study to dissect immunity to SARS-CoV-2 in a neonate nonhuman primate model. *Front. Immunol.* **13**:855230.
78. Fardoos, R. et al. HIV infection drives interferon signaling within intestinal SARS-CoV-2 target cells. *JCI Insight* **6**, e148920 (2021).
79. Olivo, A. et al. Detection of SARS-CoV-2 in subcutaneous fat but not visceral fat, and the disruption of fat lymphocyte homeostasis in both fat tissues in the macaque. *Commun. Biol.* **5**, 542 (2022).
80. Radulovic, K. & Niess, J. H. CD69 is the crucial regulator of intestinal inflammation: a new target molecule for IBD treatment? *J. Immunol. Res.* **2015**:497056.
81. Yu, L. et al. CD69 enhances immunosuppressive function of regulatory T-cells and attenuates colitis by prompting IL-10 production. *Cell Death Dis.* **9**, 905 (2018).
82. Mackay, L. K. et al. Cutting edge: CD69 interference with sphingosine-1-phosphate receptor function regulates peripheral T cell retention. *J. Immunol.* **194**, 2059–2063 (2015).
83. Chen, Z. Y. et al. Decreased expression of CD69 on T cells in tuberculosis infection resisters. *Front. Microbiol.* **11**, 1901 (2020).
84. Schlecht, G. et al. Murine plasmacytoid dendritic cells induce effector/memory CD8+ T-cell responses in vivo after viral stimulation. *Blood* **104**, 1808–1815 (2004).
85. Fonteneau, J. F. et al. Activation of influenza virus–specific CD4+ and CD8+ T cells: a new role for plasmacytoid dendritic cells in adaptive immunity. *Blood* **101**, 3520–3526 (2003).
86. Loré, K. et al. Toll-like receptor ligands modulate dendritic cells to augment cytomegalovirus-and HIV-1-specific T cell responses. *J. Immunol.* **171**, 4320–4328 (2003).
87. Fitzgerald-Bocarsly, P., Dai, J. & Singh, S. Plasmacytoid dendritic cells and type I IFN: 50 years of convergent history. *Cytokine Growth Factor Rev.* **19**, 3–19 (2008).
88. Daissormont, I. T. et al. Plasmacytoid dendritic cells protect against atherosclerosis by tuning T-cell proliferation and activity. *Circ. Res.* **109**, 1387–1395 (2011).
89. Lippens, C. et al. IDO-orchestrated crosstalk between pDCs and Tregs inhibits autoimmunity. *J. Autoimmun.* **75**, 39–49 (2016).
90. Kempski, J., Brockmann, L., Gagliani, N. & Huber, S. T(H)17 cell and epithelial cell crosstalk during inflammatory bowel disease and carcinogenesis. *Front. Immunol.* **8**, 1373 (2017).
91. Xu, H. & Wang Th17 cells coordinate with Th22 cells in maintaining homeostasis of intestinal tissues and both are depleted in SIV-infected macaques. *J. AIDS Clin. Res.* **5**, 302 (2014).
92. Klatt, N. R. & Brenchley, J. M. Th17 Cell Dynamics in HIV Infection. *Curr. Opin. HIV AIDS* **5**, 135–140 (2010).
93. Brenchley, J. M. et al. Microbial translocation is a cause of systemic immune activation in chronic HIV infection. *Nat. Med.* **12**, 1365–1371 (2006).

94. Raffatellu, M. et al. Simian immunodeficiency virus-induced mucosal interleukin-17 deficiency promotes Salmonella dissemination from the gut. *Nat. Med.* **14**, 421–428 (2008).
95. Mowat, A. M. & Agace, W. W. Regional specialization within the intestinal immune system. *Nat. Rev. Immunol.* **14**, 667–685 (2014).
96. Desalegn, G. & Pabst, O. Inflammation triggers immediate rather than progressive changes in monocyte differentiation in the small intestine. *Nat. Commun.* **10**, 3229 (2019).
97. Grainger, J. R., Konkel, J. E., Zangerle-Murray, T. & Shaw, T. N. Macrophages in gastrointestinal homeostasis and inflammation. *Pflugers Arch.* **469**, 527–539 (2017).
98. Zigmond, E. et al. Macrophage-restricted interleukin-10 receptor deficiency, but not IL-10 deficiency, causes severe spontaneous colitis. *Immunity* **40**, 720–733 (2014).
99. Bernardo, D. et al. Human intestinal pro-inflammatory CD11c(high)CCR2(+) CX3CR1(+) macrophages, but not their tolerogenic CD11c(-)CCR2(-)CX3CR1(-) counterparts, are expanded in inflammatory bowel disease. *Mucosal Immunol.* **11**, 1114–1126 (2018).
100. Kayama, H. et al. Intestinal CX3C chemokine receptor 1(high) (CX3CR1(high)) myeloid cells prevent T-cell-dependent colitis. *Proc. Natl Acad. Sci. U. S. A.* **109**, 5010–5015 (2012).
101. Shaw, M. H., Kamada, N., Kim, Y. G. & Núñez, G. Microbiota-induced IL-1β, but not IL-6, is critical for the development of steady-state TH17 cells in the intestine. *J. Exp. Med.* **209**, 251–258 (2012).
102. Das, A. et al. Monocyte and macrophage plasticity in tissue repair and regeneration. *Am. J. Pathol.* **185**, 2596–2606 (2015).
103. Pull, S. L., Doherty, J. M., Mills, J. C., Gordon, J. I. & Stappenbeck, T. S. Activated macrophages are an adaptive element of the colonic epithelial progenitor niche necessary for regenerative responses to injury. *Proc. Natl Acad. Sci. U. S. A.* **102**, 99–104 (2005).
104. Hadis, U. et al. Intestinal tolerance requires gut homing and expansion of FoxP3+ regulatory T cells in the lamina propria. *Immunity* **34**, 237–246 (2011).
105. Li, J. et al. Dynamic role of macrophage CX3CR1 expression in inflammatory bowel disease. *Immunol. Lett.* **232**, 39–44 (2021).
106. Kamada, N. et al. Unique CD14 intestinal macrophages contribute to the pathogenesis of Crohn disease via IL-23/IFN-gamma axis. *J. Clin. Invest.* **118**, 2269–2280 (2008).
107. Grimm, M. C. et al. Direct evidence of monocyte recruitment to inflammatory bowel disease mucosa. *J. Gastroenterol. Hepatol.* **10**, 387–395 (1995).
108. Kim, M. et al. Critical role for the microbiota in CX3CR1+ intestinal mononuclear phagocyte regulation of intestinal T cell responses. *Immunity* **49**, 151–163.e5 (2018).
109. Kim, M., Hill, A. A., Wu, W. J. & Diehl, G. E. Intestinal microbes direct CX 3 CR1 + cells to balance intestinal immunity. *Gut Microbes* **10**, 540–546 (2019).
110. Diehl, G. E. et al. Microbiota restricts trafficking of bacteria to mesenteric lymph nodes by CX3CR1hi cells. *Nature* **494**, 116–120 (2013).
111. Prasad, R. et al. Plasma microbiome in COVID-19 subjects: an indicator of gut barrier defects and dysbiosis. *Int. J. Mol. Sci.* **23**, 9141 (2022).
112. Sokol, H. et al. SARS-CoV-2 infection in nonhuman primates alters the composition and functional activity of the gut microbiota. *Gut Microbes* **13**, 1–19 (2021).
113. Saia, R. S. et al. Clinical investigation of intestinal fatty acid-binding protein (I-FABP) as a biomarker of SARS-CoV-2 infection. *Int. J. Infect. Dis.* **113**, 82–86 (2021).
114. Shive, C. L., Jiang, W., Anthony, D. D. & Lederman, M. M. Soluble CD14 is a nonspecific marker of monocyte activation. *AIDS* **29**, 1263–1265 (2015).
115. Silvin, A. et al. Elevated calprotectin and abnormal myeloid cell subsets discriminate severe from mild COVID-19. *Cell* **182**, 1401–1418.e18 (2020).
116. Miyakawa, K. et al. Reduced replication efficacy of severe acute respiratory syndrome coronavirus 2 omicron variant in "Mini-gut" Organoids. *Gastroenterology* **163**, 514–516 (2022).
117. Fernández-de-Las-Peñas, C. et al. Post-COVID-19 symptoms 2 years after SARS-CoV-2 infection among hospitalized vs nonhospitalized patients. *JAMA Netw. Open* **5**, e2242106 (2022).
118. Yang, W. et al. Clinical characteristics of 310 SARS-CoV-2 Omicron variant patients and comparison with Delta and Beta variant patients in China. *Virol. Sin.* **37**, 704–715 (2022).
119. Pivonello, R. et al. Sex disparities in COVID-19 severity and outcome: are men weaker or women stronger? *Neuroendocrinology* **111**, 1066–1085 (2021).
120. Johnson, L., Shapiro, M., Janicki, S., Mankoff, J. & Stricker, R. B. Does biological sex matter in Lyme disease? The need for sex-disaggregated data in persistent illness. *Int. J. Gen. Med.* **16**, 2557–2571 (2023).
121. Tharakan, T. et al. Are sex disparities in COVID-19 a predictable outcome of failing men's health provision? *Nat. Rev. Urol.* **19**, 47–63 (2022).
122. Marlin, R. et al. Antiviral efficacy of favipiravir against Zika and SARS-CoV-2 viruses in non-human primates. *Nat. Commun.* **13**, 5108 (2022).
123. WHO protocol for detection of SARS-CoV-2. Available at: https://www.who.int/docs/default-source/coronaviruse/real-time-rt-pcr-assays-for-the-detection-of-sars-cov-2-institut-pasteur-paris.pdf [Date accessed: XXX].
124. Dagotto, G. et al. Comparison of subgenomic and total RNA in SARS-CoV-2 challenged rhesus macaques. *J. Virol.* **95**, e02370–e2420 (2021).
125. Brouwer, P. J. M. et al. Two-component spike nanoparticle vaccine protects macaques from SARS-CoV-2 infection. *Cell* **184**, 1188–1200.e19 (2021).
126. Marlin, R. et al. Targeting SARS-CoV-2 receptor-binding domain to cells expressing CD40 improves protection to infection in convalescent macaques. *Nat. Commun.* **12**, 5215 (2021).